

THE CALIBRATION OF A PORTABLE INDUCTION
MAGNETOMETER SYSTEM

by

Liana Zambresky
B.Sc., University of Redlands, 1973

A THESIS SUBMITTED IN PARTIAL FULFILMENT OF
THE REQUIREMENTS FOR THE DEGREE OF
MASTER OF SCIENCE

in the Department
of
Geophysics and Astronomy

We accept this thesis as conforming to the
required standard

The University of British Columbia
June 1977

© Liana Francesk Zambresky, 1977

In presenting this thesis in partial fulfilment of the requirements for an advanced degree at the University of British Columbia, I agree that the Library shall make it freely available for reference and study.

I further agree that permission for extensive copying of this thesis for scholarly purposes may be granted by the Head of my Department or by his representatives. It is understood that copying or publication of this thesis for financial gain shall not be allowed without my written permission.

Department of Geophysics + Astronomy

The University of British Columbia
2075 Wesbrook Place
Vancouver, Canada
V6T 1W5

Date July 8, 1977

ABSTRACT

An investigation made concerning the characteristics of a sensor coil for an induction magnetometer shows that it is feasible to make the first stage 60 Hertz rejection filter of the Butterworth type. This is an improvement in design over the Twin-T filter which is sometimes used as a first stage filter as the number of electrical components is reduced and there is no possibility of ringing between the coil inductor and the filter capacitors.

Two methods of relative calibration for the induction magnetometer system give reliable response curves. One method uses a Wheatstone bridge. The sensor is one arm of the bridge and it is shown that the effect of the signal generator is the same as if the coil was excited by a natural event. The second method involves exciting the sensor by a field created by a small secondary coil. The agreement between the two methods is good.

An experimental approach to the absolute calibration is successfully carried out by comparing the output from the uncalibrated system to an air core system which has been previously calibrated. A theoretical approach is used to give a good indication of the sensitivity of the sensor coil. The sensitivity is dependent primarily upon the turn number and the length of the coil.

TABLE OF CONTENTS

ABSTRACT		ii
LIST OF FIGURES		v
LIST OF TABLES		viii
ACKNOWLEDGEMENTS		ix
CHAPTER I	GENERAL INTRODUCTION	1
CHAPTER II-1	THE 60 HERTZ REJECTION PROBLEM	6
II-1	Introduction	6
II-2	Theory of Twin-T filter	7
II-2.1	Computer Results	15
II-3	Theory of Butterworth filter	17
II-3.1	Laboratory Results	22
CHAPTER III	THEORY OF THE BRIDGE METHOD	25
III-1	Introduction	25
III-2	An Intuitive Approach Using the Norton Equivalent	26
III-2.1	Theory at Higher Frequencies	29
III-3	Theory of the Bridge Method	33
III-3.1	Case of Observation	37
III-3.2	Case of Calibration	37
III-3.3	Computer and Laboratory Results	40
III-4	The Case of Observation with and Without the Bridge	46

CHAPTER IV	THEORY OF THE SECONDARY COIL METHOD	52
IV-1	Introduction	52
IV-2	Theory of Operation	53
IV-3	Theory of Calibration	56
CHAPTER V	THE ABSOLUTE CALIBRATION	66
V-1	A Laboratory Approach	66
V-2	A Theoretical Approach to the Absolute Sensitivity	74
CHAPTER VI	SUMMARY AND CONCLUDING REMARKS	81
APPENDIX 1	Methods of Determining the Inductance and Capacitance of a Coil with Finite Resistance	83
APPENDIX 2	The Transfer Function of the Amplifier System	88
APPENDIX 3	The Transfer Function for the Third Order Low Pass Filter	91
APPENDIX 4	REFERENCES ON THE ABSOLUTE CALIBRATION According to the Bridge Method	93
LIST OF REFERENCES CONSULTED		95

List of Figures

Chapter I

Fig. 1-1	Equivalent circuit of sensor coil	2
----------	-----------------------------------	---

Chapter II

Fig. 2.2-1	The symmetric Twin-T filter	7
Fig. 2.2-2	Block diagram of sensor coil/Twin-T network	12
Fig. 2.2.1-1	Computer simulation of the frequency response of the coil/Twin-T sensing system	16
Fig. 2.3-1	An analog Butterworth filter	17
Fig. 2.3-2	The transfer function for the Butterworth filter	20
Fig. 2.3.1-1	Laboratory set-up for the Butterworth filter	22
Fig. 2.3.1-2	Butterworth filter characteristics of the sensor coil system	24

Chapter III

Fig. 3.2-1	The Wheatstone bridge	26
Fig. 3.2-2	Norton equivalent of the sensor coil	28
Fig. 3.2.1-1	Wheatstone bridge at higher frequencies	29
Fig. 3.2.1-2	Norton equivalent of the Wheatstone bridge	30
Fig. 3.2.1-3	Circuit used to derive a new Norton equivalent	30
Fig. 3.3-1	The bridge circuit with parameters as they are defined for circuit analysis	34

Fig. 3.3.3-1	Computer simulation to determine the effect of the conditions $R_4 \gg R_1$ and $R_3 \gg R_2$ on the response of the magnetometer system when using the bridge method	41
Fig. 3.3.3-2	The laboratory bridge circuit	43
Fig. 3.3.3-3	The normalized amplitude response of the magnetometer system according to the bridge method	44
Fig. 3.3.3-4	The phase response of the magnetometer system according to the bridge method	45
Fig. 3.4-1	Diagram of sensor coil and load impedance	47
Fig. 3.4-2	The essential elements of the bridge circuit	50
Fig. 3.4-3	The effect of the resistance R_4 on the frequency response as obtained from the bridge method	51

Chapter IV

Fig. 4.2-1	The secondary coil method at the time of operation	53
Fig. 4.3-1	The secondary coil method at the time of calibration	56
Fig. 4.3-2	The secondary coil method in the laboratory	60
Fig. 4.3-3	The normalized amplitude response of the magnetometer system according to the secondary coil method	62
Fig. 4.3-4	The phase response of the magnetometer system according to the secondary coil method	63
Fig. 4.3-5	A comparison of the frequency response curves obtained in the laboratory from the secondary coil method and the bridge method	64

Fig. 4.3-6	A comparison of the phase response curves obtained in the laboratory from the secondary coil method and the bridge method	65
<u>Chapter V</u>		
Fig. 5.1-1	Circuit diagram for the air core system	69
Fig. 5.1-2	Computer simulated frequency response of the air core coil system	71
Fig. 5.1-3	Method to determine the inner radius of a large coil	72
Fig. 5.1-4	The micropulsation event used for the absolute calibration	73
Fig. 5.2-1	The dependence of the geometric permeability μ , upon the ratio of the lengths of the semiprinciple axes of a prolate spheroid, a/b	80
<u>Appendix 1</u>		
Fig. A.1-1	Equivalent circuit of a sensor coil	83
Fig. A.1-2	First method of determining L	84
Fig. A.1-3	Second method of determining L	85
Fig. A.1-4	The anti-resonance point	86
<u>Appendix 2</u>		
Fig. A.2-1	Mu-metal core amplifier system	89
Fig. A.2-2	Transfer function for filters of the Mu-metal core amplifier system	90
<u>Appendix 3</u>		
Fig. A.3-1	The third order low pass filter	91

List of TablesChapter I

Table I-1	Coil specifications	5
-----------	---------------------	---

ACKNOWLEDGEMENTS

I would like to express my sincere gratitude and appreciation to Dr. Tomiya Watanabe for his continuous help and guidance as my research advisor throughout the work presented in this thesis.

I gratefully acknowledge Dr. R.D. Russell for many helpful discussions and ideas.

I would like to express many thanks to Dr. K. Hayashi and Dr. T. Oguti for their patient guidance in the electronics laboratory.

I would like to acknowledge the Victoria Geophysical Observatory, Dept. of Energy, Mines and Resources for equipment which we borrowed.

For the operation at Churchill, Manitoba, I would like to thank Mr. C.R. Barrett, superintendent and his staff at the Churchill Research Range of NRC.

This research received financial support from the following grants :

NRC A-3564

NRC E-2923

DRB 9511-112

UBC Arctic and Alpine Research Committee 65-0444

NRC D-6409

UBC Summer Research Scholarship

CHAPTER I

GENERAL INTRODUCTION

Recently, a portable induction magnetometer system was designed by the aeronomy group at the University of British Columbia. It is the long term intent of this group to establish a number of observing stations across northern Canada for micropulsation research. It was felt that a system could be built at a cost significantly less than commercial magnetometers. The requirements of this instrument are such that it should cover the frequency band from 0.002 Hz to 4 Hz and take the signal level from the order of milligamma to ten gammas. The sensor was constructed with a Mu-metal core in order to reduce the physical size from that of an air core sensor. Mu-metal is a high permeability alloy of nickel and iron with a small amount of chromium and molybdenum. Ueda (1975) demonstrated that the Mu-metal core does not cause significant distortions or harmonics to the signal contrary to what some earlier investigators had thought.

The equivalent circuit which is used for the sensor coil throughout this research is shown in Fig. 1-1. The capacitance effect of the windings, noted as early as 1910 from general antenna use, Campbell (1969), gives rise to the capacitor which is parallel to the resistance and inductance of the coil. The voltage generator, V , arises from the current which is induced in the coil by the changing magnetic flux.

It is difficult to measure the coil inductance and capacitance using a bridge which is designed for measuring pure inductance and capacitance. For this reason, somewhat laborious methods must be put into practice. A compilation of such methods used for this research is given in Appendix A-1. These methods lend a great amount of credibility to the equivalent circuit concept because the coil was found to behave exactly as the circuit theory predicts in each method.

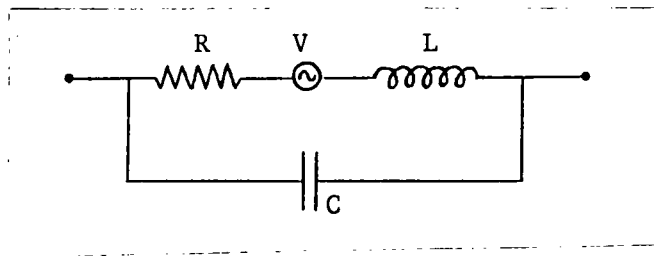


Fig. 1-1 Equivalent Circuit of Sensor Coil

Further support for the equivalent circuit occurs from observations that the output of the sensor coil with a parallel resistor and capacitor of appropriate values has characteristics of a Butterworth filter. The theory of the Butterworth filter is developed in detail according to circuit theory. Laboratory results concur with theory and give more support to Fig. 1-1. A useful improvement in the design of a 60 Hz rejection filter results from this analysis which is discussed in detail in Chapter II.

The primary intent of this thesis is to investigate the practicality of two methods of relative calibration for

finding the frequency response of the induction magnetometer. One of these methods is called the bridge method in which one arm of a Wheatstone bridge circuit is the sensor coil of the magnetometer. It will be shown that emf generated in the sensor coil by an external time-varying magnetic field can be simulated by driving the bridge with a signal generator. The other method, called the secondary coil method, is one in which a small secondary coil is wound on the core coaxially with the sensor coil and creates magnetic flux to be detected by the sensor coil.

The secondary coil method has the disadvantage that an extra cable is needed between the secondary coil and the amplifier system. In the field, the coils and the amplifier electronics are separated by approximately 100 yards in order to prevent spurious noise generated by the electronics from being mixed with the natural signal. Thus, it would be better to have one cable instead of two, not only from the standpoint of cost and convenience, but also because the possibility of undesirable cable effects would be reduced, i.e. "cross-talk". This problem makes the bridge method more desirable as a calibration procedure.

An absolute calibration must be carried out in order to determine the level of the relative frequency response curve. This is done by comparing the output of the Mu-metal core system to another system which is already calibrated. This second system is an air core magnetometer. Sensitivity of an air core coil can be calculated exactly knowing the

geometry of the coil and its turn number. The two magnetometers are set up in the field, approximately 100 yards apart, and record micropulsations. The assumption is made that such a global event will not change over this distance. Some micropulsation events are recorded as sinusoidal signals and it is this type of event which is used for the comparison. Readings can be made over a number of cycles so that the error of this measurement is small.

Finally, a theoretical approach is taken towards the sensitivity of a coil in order to elucidate which parameters are significant. The parameters of interest are the coil dimensions, the gauge of the wire out of which the windings are made, and the permeability of the core. Such an approach would be helpful when designing new sensors.

The specifications of all of the coils used for this research are given in Table I-1. These specifications will be referenced throughout this thesis.

	Turn Number	R (Ω)	L (H)	C	Inner Diam. (cm)	Outer Diam. (cm)	Length (cm)
Air Core Coil	5000	5130	120	.50 μ f	149.02	151.40	4.76
Mu-metal Core Coil (1976)	50,000	1831	930	.188 μ f	3.17	7.30	45.72
Secondary Coil	20	-----	.011	-----	3.17	-----	-----
Calibration Coil	1000	11	-----	-----	17.14	-----	241.3
Mu-metal Core Coil (1975)	50,000	2230	1050	.048 nf	4.00	9.5	35.56

Table I-1 Coil Specifications

CHAPTER II

THE 60 HERTZ REJECTION PROBLEM

II-1 Introduction

The rejection of 60 Hz noise is a problem which requires careful consideration for a magnetometer that is being designed to detect micropulsations. At low noise sites which are carefully chosen in the field, the noise is considerably reduced from what it would be in a city. It is necessary to reduce the 60 Hz noise by at least a factor of 100 before allowing the signal to be amplified. Otherwise the amplifier may be overloaded or the micropulsation information lost due to the extremely low signal to noise ratio.

One method which has been used for some previous magnetometers is to place a Twin-T filter, a notch filter with center frequency at 60 Hz, directly between the sensor coil and the amplifier. It will be shown in the discussion which follows that the frequency response of the signal output from the Twin-T filter is dependent upon the input impedance of the amplifier. This is not a desirable effect.

There is a different approach to the first stage of the 60 Hz rejection problem that is better for two reasons. One reason is that the frequency response in the micropulsation range is ensured to be flat. The other is that only one resistor and capacitor are needed instead of six carefully matched components for a Twin-T filter. This approach

requires making the sensor coil and the parallel RC combination into an analog Butterworth filter.

II-2 Theory of Twin-T Filter

The filter of interest is the symmetric Twin-T. A circuit diagram is shown in Fig. 2.2-1.

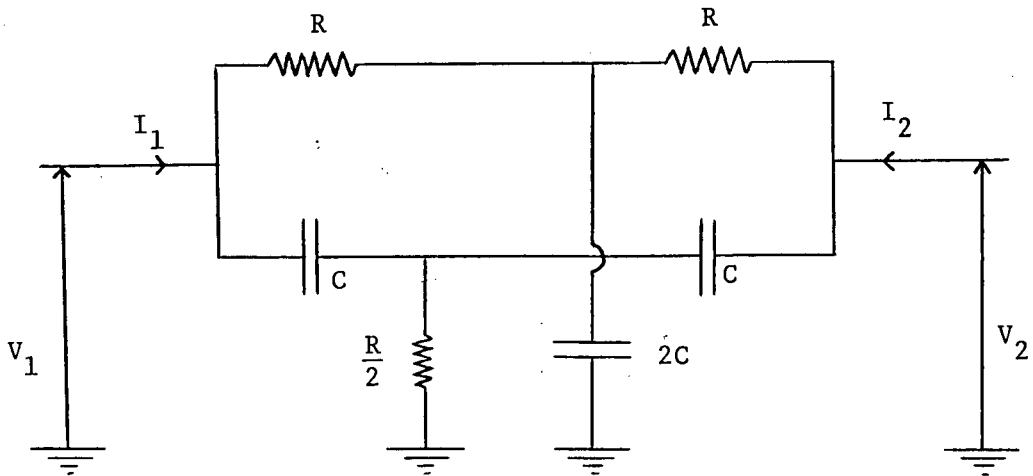
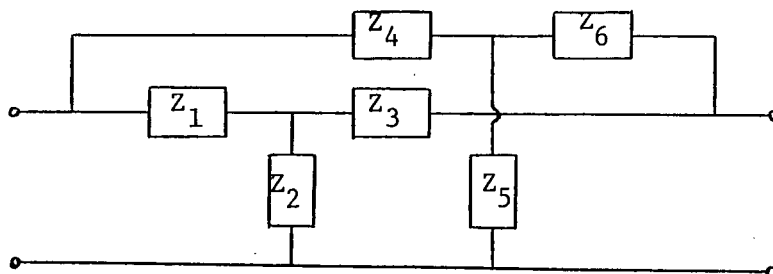
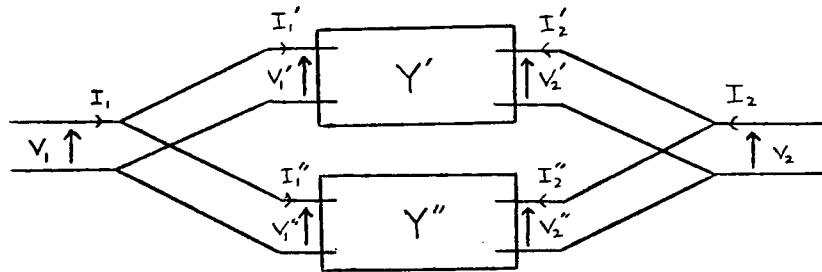


Fig. 2.2-1 The symmetric Twin-T filter

To aid making a circuit analysis, the circuit is generalized to that of:



This is a parallel connection of two networks and may be depicted schematically as:

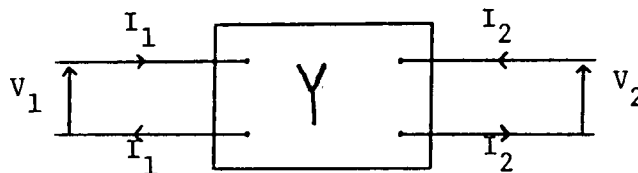


Each network may be described by a matrix equation in current, admittance and voltage,

$$\underline{I}' = \underline{Y}' \underline{V}'$$

$$\underline{I}'' = \underline{Y}'' \underline{V}''$$

To describe the network as a whole, consider the figure:



Then:

$$\underline{I} = \underline{I}' + \underline{I}''$$

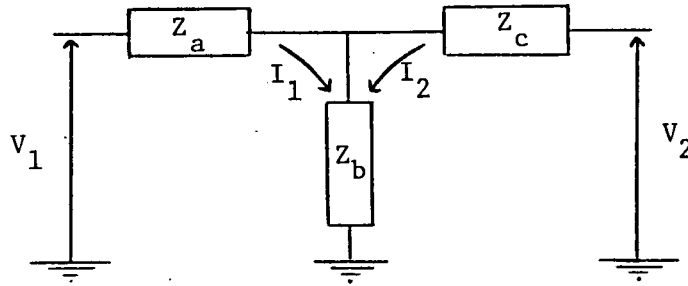
$$\underline{V} = \underline{V}' = \underline{V}''$$

This leads to the desired result:

$$\underline{I} = (\underline{Y}' + \underline{Y}'') \underline{V}$$

This last equation is important because it means that the admittance matrix of a number of networks connected in

parallel is the sum of the admittance matrix of each individual network. In the case of the parallel-T network, the entire network can be broken down into two simpler networks of the type:



The mesh equations for this network are:

$$V_1 = (Z_a + Z_b)I_1 + Z_b I_2$$

$$V_2 = Z_b I_1 + (Z_b + Z_c)I_2$$

The matrix representation which follows is:

$$\begin{pmatrix} V_1 \\ V_2 \end{pmatrix} = \begin{pmatrix} Z_a + Z_b & Z_b \\ Z_b & Z_b + Z_c \end{pmatrix} \begin{pmatrix} I_1 \\ I_2 \end{pmatrix}$$

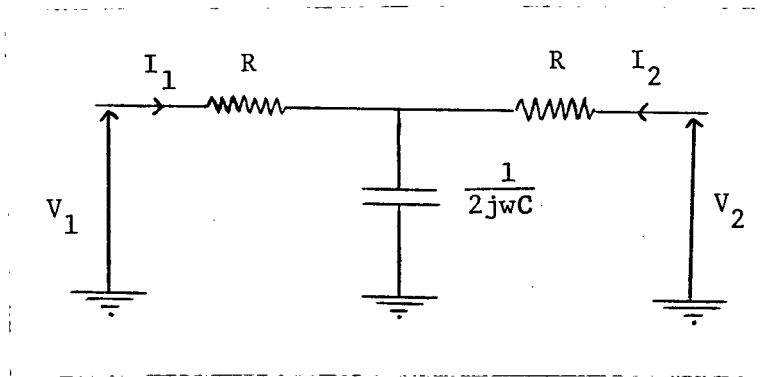
Or, more generally:

$$\begin{pmatrix} V_1 \\ V_2 \end{pmatrix} = \begin{pmatrix} Z_{11} & Z_{12} \\ Z_{21} & Z_{22} \end{pmatrix} \begin{pmatrix} I_1 \\ I_2 \end{pmatrix}$$

It is of interest to have the matrix equations in the form $\underline{I} = \underline{Y}\underline{V}$. The \underline{Y} matrix, or the admittance matrix, is the inverse of the \underline{Z} matrix. Thus, $\underline{I} = \underline{Y}\underline{V}$ implies:

$$\begin{pmatrix} I_1 \\ I_2 \end{pmatrix} = \frac{1}{|Z|} \begin{pmatrix} Z_{22} & -Z_{12} \\ -Z_{21} & Z_{11} \end{pmatrix} \begin{pmatrix} V_1 \\ V_2 \end{pmatrix}$$

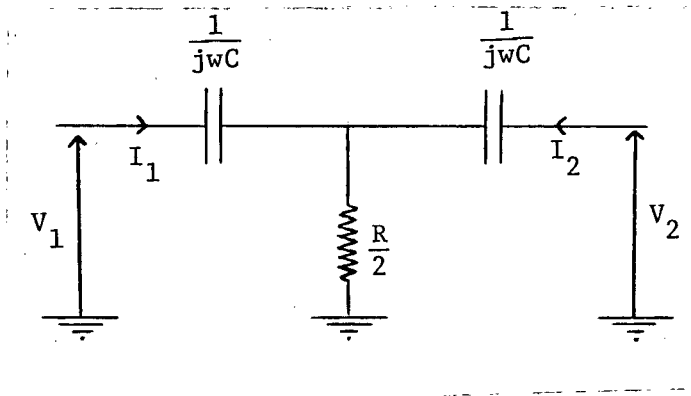
$|Z|$ is the determinant of the \underline{Z} matrix. It is necessary to determine the \underline{Y} matrix for each of the parallel-T sub-networks. The first network to consider is:



The resulting \underline{Y} matrix is:

$$\underline{Y}' = \frac{jwC}{R(1+jwCR)} \begin{pmatrix} R + \frac{1}{2jwC} & -\frac{1}{2jwC} \\ -\frac{1}{2jwC} & R + \frac{1}{2jwC} \end{pmatrix}$$

The second network to consider is:



This has the \underline{Y} matrix:

$$\underline{Y}'' = \frac{-\omega^2 C^2}{1+j\omega CR} \begin{pmatrix} \frac{R}{2} + \frac{1}{j\omega C} & -\frac{R}{2} \\ -\frac{R}{2} & \frac{R}{2} + \frac{1}{j\omega C} \end{pmatrix}$$

The \underline{Y} matrix for the entire parallel-T network as depicted in Fig. 2.2-1 is then $\underline{Y} = \underline{Y}' + \underline{Y}''$. This matrix is:

$$\underline{Y} = \begin{pmatrix} Y_{11} & Y_{12} \\ Y_{12} & Y_{11} \end{pmatrix} \quad 2.2-1$$

$$\text{where: } Y_{11} = \frac{1 + 4j\omega CR + (j\omega CR)^2}{2R(1+j\omega CR)}$$

$$Y_{12} = -\frac{1 + (j\omega CR)^2}{2R(1+j\omega CR)}$$

The ultimate aim of this discussion is to find the frequency response of the Twin-T network when it has a signal from the sensor as input and when it is terminated by the finite impedance of the amplifier system. Schematically, this is depicted by Fig 2.2-2. The matrix equation describing this system is:

$$\begin{pmatrix} V_1 \\ I_1 \end{pmatrix} = \begin{pmatrix} A_1 & B_1 \\ C_1 & D_1 \end{pmatrix} \begin{pmatrix} A_2 & B_2 \\ C_2 & D_2 \end{pmatrix} \begin{pmatrix} V_3 \\ I_3 \end{pmatrix}$$

$$\begin{pmatrix} V_1 \\ I_1 \end{pmatrix} = \begin{pmatrix} A_1 A_2 + B_1 C_2 & A_1 B_2 + B_1 D_2 \\ C_1 A_2 + D_1 C_2 & C_1 B_2 + D_1 D_2 \end{pmatrix} \begin{pmatrix} V_3 \\ I_3 \end{pmatrix}$$

$$= \begin{pmatrix} A' & B' \\ C' & D' \end{pmatrix} \begin{pmatrix} V_3 \\ I_3 \end{pmatrix}$$

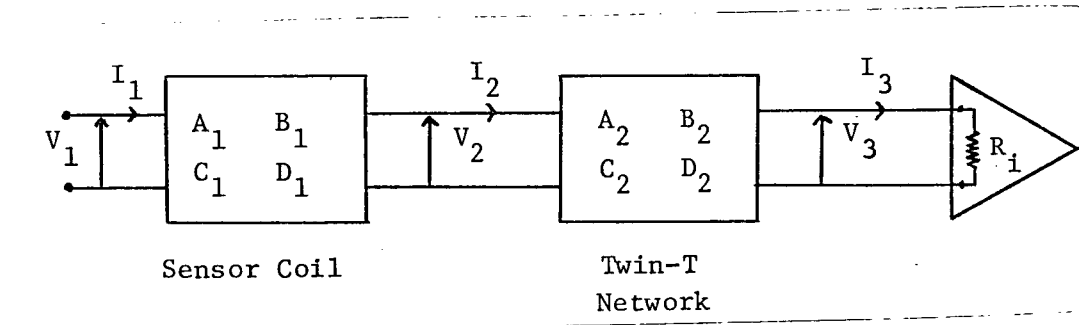


Fig. 2.2-2

From the matrix equation, it follows that $V_1 = A' V_3 + B' I_3$ and since $I_3 = V_3 / R_i$, the resulting transfer function is:

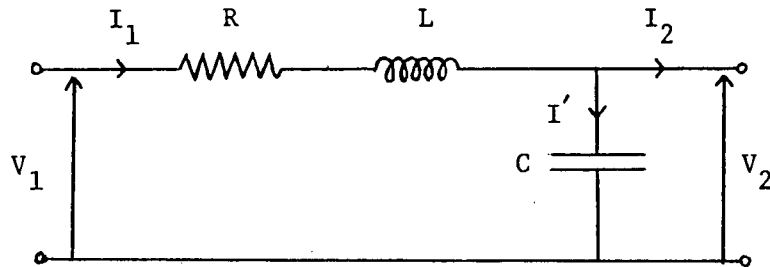
$$\frac{V_3}{V_1} = \frac{R_i}{A' R_i + B'}$$

The matrices depicted above are not in the form of the Y matrix. In the terminology of electrical engineering these have the form of the F matrix. The required transformation is:

$$\underline{F} = \begin{pmatrix} A_2 & B_2 \\ C_2 & D_2 \end{pmatrix} = \begin{pmatrix} -\frac{Y_{22}}{Y_{21}} & -\frac{1}{Y_{21}} \\ -\frac{|Y|}{Y_{21}} & -\frac{Y_{11}}{Y_{21}} \end{pmatrix}$$

where: $|Y| = Y_{11} Y_{22} - Y_{12} Y_{21}$

To compute the F matrix for the sensor coil, consider the following circuit diagram:



From the RLC loop, an equation can be derived for I_1 .

$$I_1 = j\omega C V_2 + I_2$$

From the potential drop across R and L:

$$I_1 = \frac{V_1 - V_2}{R + j\omega L}$$

This leads to the expression for V_1 :

$$V_1 = (1 - \omega^2 LC + j\omega CR) V_2 + (R + j\omega L) I_2$$

The sensor coil matrix is then:

$$\begin{pmatrix} A_1 & B_1 \\ C_1 & D_1 \end{pmatrix} = \begin{pmatrix} 1 - \omega^2 LC + j\omega CR & R + j\omega L \\ j\omega C & 1 \end{pmatrix}$$

Now all of the quantities to determine the complete transfer function of the system in Fig. 2.2-2 are known. The final result is:

$$\frac{V_3}{V_1} = \frac{R_i}{A' R_i + B'}$$

2.2-2)

where:

$$A' = A_1 A_2 + B_1 C_2$$

$$B' = A_1 B_2 + B_1 D_2$$

$$A_1 = 1 - \omega^2 LC + j\omega CR$$

$$B_1 = R + j\omega L$$

$$A_2 = -\frac{Y_{11}}{Y_{12}}$$

$$B_2 = -\frac{1}{Y_{12}}$$

$$C_2 = \frac{Y_{12}^2 - Y_{11}^2}{Y_{12}}$$

$$D_2 = -\frac{Y_{11}}{Y_{12}}$$

Y_{11} , Y_{12} are defined by 2.2-1

II-2.1 Computer Results

A computer program was written to compute the transfer function of equation 2.2-2. The results of this computing may be seen in Fig. 2.2.1-1. The striking feature to notice is how the shape of the transfer function changes as a function of the terminating impedance of the Twin-T network. This terminating impedance is the input impedance to the amplifier system. If the amplifier is an integrated circuit, then its input impedance could easily be of the order of $10M\Omega$ and a severe ringing effect will occur near 5 Hz. This ringing is the result of coupling between the coil inductor and the Twin-T capacitors. If the amplifier input impedance can be reduced, then the ringing effect will lessen. The curve for an input impedance of $7.5 K\Omega$ shows no ringing at all and has a smooth drop off. However, as described earlier, such a response curve can be obtained by exploiting a Butterworth filter. It would require only one resistor and capacitor in parallel to the coil. The Twin-T would require six carefully matched resistors and capacitors, and in the case of balanced input, twelve elements would have to be matched instead of six. In practice, this may be a troublesome requirement. It should also be noticed that as the terminating impedance is reduced, the sensitivity at the lower frequencies is reduced. This is not a desirable effect.

II-3 Theory of the Butterworth Filter

The theory will now be developed for an analog Butterworth filter. The circuit to be analyzed is shown in Fig. 2.3-1. A resistor and capacitor are placed parallel to the output of the sensor coil.

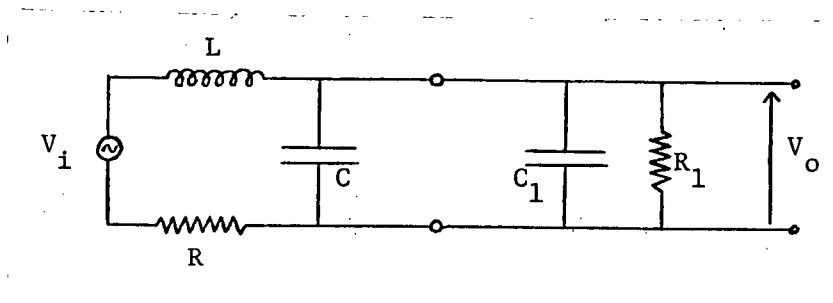


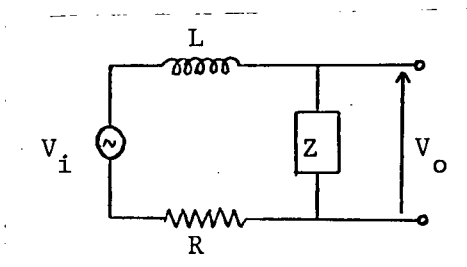
Fig.2.3-1 An Analog Butterworth Filter

To determine V_o , first find the equivalent impedance of the three parallel quantities C , C_1 , and R_1 .

$$\frac{1}{Z} = j\omega C + j\omega C_1 + \frac{1}{R_1}$$

$$Z = \frac{R_1}{1 + j\omega(C + C_1)R_1}$$

The equivalent circuit becomes:



V_o can now be found from the voltage divider method.

$$V_o = \frac{Z}{R + j\omega L + Z} V_i$$

After substituting for Z , a considerable amount of algebra leads to the result:

$$V_o = \frac{V_i e^{-i\theta}}{\left[\left(1 + \frac{R}{R_1}\right)^2 + \left\{ (C+C_1)^2 R^2 + \left(\frac{L}{R_1}\right)^2 - 2L(C+C_1) \right\} \omega^2 + L^2 (C+C_1)^2 \omega^4 \right]^{1/2}} \quad 2.3-1$$

$$\theta = \tan^{-1} \left\{ \frac{\omega \left[(C+C_1)R + \frac{L}{R_1} \right]}{\left(1 + \frac{R}{R_1}\right) - \omega^2 L (C+C_1)} \right\}$$

This equation for V_o can be put into a non-dimensional form. The following substitutions will be made:

1. Let α represent the ratio of d.c. resistance of the sensor coil to the terminating resistance.

$$\alpha = \frac{R}{R_1} \quad 2.3-2$$

2. Let β represent the inverse Q factor of the R-L-C series circuit.

$$\beta = \frac{1}{Q} = R \sqrt{(C+C_1)/L} \quad 2.3-3$$

3. Let f_r represent the resonance frequency of the R-L-C series circuit.

$$f_r = \frac{1}{2\pi \sqrt{L(C+C_1)}} \quad 2.3-4$$

Now equation 2.3-1 can be re-expressed as:

$$V_o = \frac{V_i e^{-i\theta}}{\left[(1+\alpha)^2 + \left(\beta^2 + \frac{\alpha^2}{\beta^2} - 2 \right) \left(\frac{f}{f_r} \right)^2 + \left(\frac{f}{f_r} \right)^4 \right]^{1/2}} \quad 2.3-5$$

where

$$\theta = \tan^{-1} \left\{ \frac{(\beta + \frac{\alpha}{\beta})(f/f_r)}{(1 + \alpha) - (f/f_r)^2} \right\}$$

In order for the circuit 2.3-1 to respond as a Butterworth filter, the term $(f/f_r)^2$ must be made to approach zero. A Butterworth filter of any order is present when the transfer function contains the following expression:

$$\left| H\left(\frac{f}{f_r}\right) \right|^2 = \frac{1}{1 + \left(\frac{f}{f_r}\right)^{2n}}$$

A plot of the transfer function for the Butterworth filter of orders $n=1,2,3$ can be seen in Fig 2.3-2. It is evident that in the case of equation 2.3-5, this is a Butterworth filter of order 2 since it is of the form:

$$\left| \frac{V_o}{V_i} \right|^2 = \frac{1}{1 + \left(\frac{f}{f_r}\right)^4} \quad 2.3-6$$

if the second term in the denominator can be made negligible.

It can be seen from the circuit diagram 2.3-1 that it would be desirable to have R_1 large compared to R as this would increase the sensitivity. Thus it can be expected that $\alpha \ll 1$. In the case that $\alpha \approx 0$, the second term vanishes for:

$$\beta = \sqrt{2}$$

In the case that $0 < \alpha < 1$, the second term vanishes for either of the following two values of β :

$$\beta = \sqrt{1 + \sqrt{1 - \alpha^2}}$$

$$\beta = \sqrt{1 - \sqrt{1 - \alpha^2}}$$

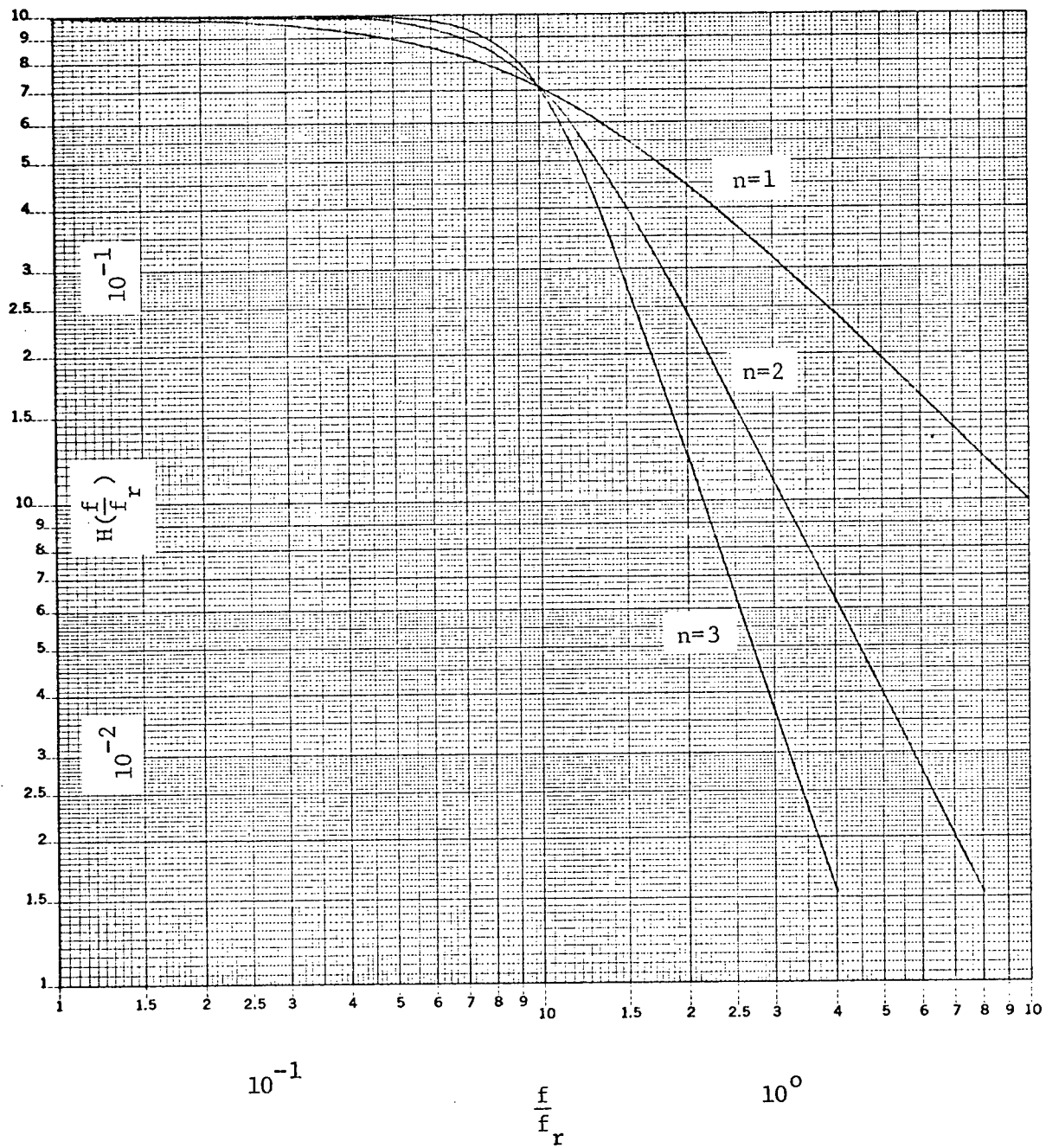


Fig. 2.3-2 The transfer function for the Butterworth filter

If $0 < \alpha \ll 1$, the binomial series expansion may be used to show that the above two values are approximately equal to:

$$\beta = \sqrt{2} \left(1 - \frac{1}{8} \alpha^2 \right)$$

$$\beta = \alpha / \sqrt{2}$$

In the case that $\alpha > 1$, there is no β which can make the second term vanish. This is another reason why α is desired to be small.

In practice, it is best to determine β first and then make α equal to that value which will nullify the second term. As the sensor will be used to detect micropulsations, it is desirable that it have a flat frequency response over the range from .002 Hz - 4 Hz. Also, since there is a considerable amount of man made noise at 60 Hz, it is necessary to optimize the qualities of the Butterworth filter in order to reduce the amount of noise picked up by the sensor. The amplitude of the 60 Hz noise can be dropped by a factor of 100 if the cut-off frequency is made equal to 6 Hz. Thus, C_1 can be determined from equation 2.3-4 provided the coil parameters R, L and C are known. This leads to:

$$C_1 = \frac{1}{L} \frac{1}{(2\pi f_c)^2} - C \quad 2.3-7$$

β can now be found from equation 2.3-3. The value of α which will nullify the second term in 2.3-5 is:

$$\alpha = \beta \sqrt{2 - \beta^2}$$

If $\beta > \sqrt{2}$, no α can make the second term vanish. β for this type of sensor is typically of the order of 10^{-4} - 10^{-2} , Ueda

and Watanabe (1975), so there is not any threat that this condition might occur. Thus, R can be found from the equation:

$$R_1 = \frac{R}{\beta \sqrt{2 - \beta^2}} \quad 2.3-8$$

II-3.1 Laboratory Results

The circuit of Fig. 2.3.1-1 was set up in the laboratory to determine whether the theory of the Butterworth filter is correct for the coils.

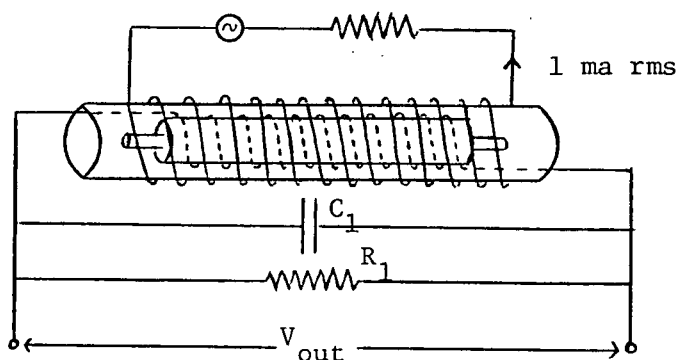


Fig. 2.3.1-1 Laboratory Set-up for the Butterworth Filter

A sinusoidal magnetic field was created inside a large calibration coil. The intensity of the field at the center of the coil is 1471 Gamma from the rms current of 1 ma that flows through its windings. The sensor coil was placed inside the large coil. The time-varying magnetic field induced a

sinusoidal emf in the sensor coil and the output from the coil was measured across a parallel RC load. From equation 2.3-7, the corner frequency of 6 Hz and the coil specifications of the Mu-metal core coil (1975), (see Table I-1), the value of the parallel capacitor was determined to be $.67 \mu\text{f}$. Then, from equation 2.3-3, $\beta = .0565$. This leads to the value $R_1 = 28\text{K}\Omega$ as determined from equation 2.3-8.

The results of the laboratory experiment can be seen in Fig. 2.3.1-2. The frequency response is flat at the lower frequencies and begins to drop off at 4 Hz. The amplitude has dropped by nearly a factor of 100 at 60 Hz. It should be noted that V_{out} in Fig 2.3.1-1 has been divided by frequency because the emf induced in a coil by a changing magnetic flux is proportional to frequency and the amplitude of the magnetic field.

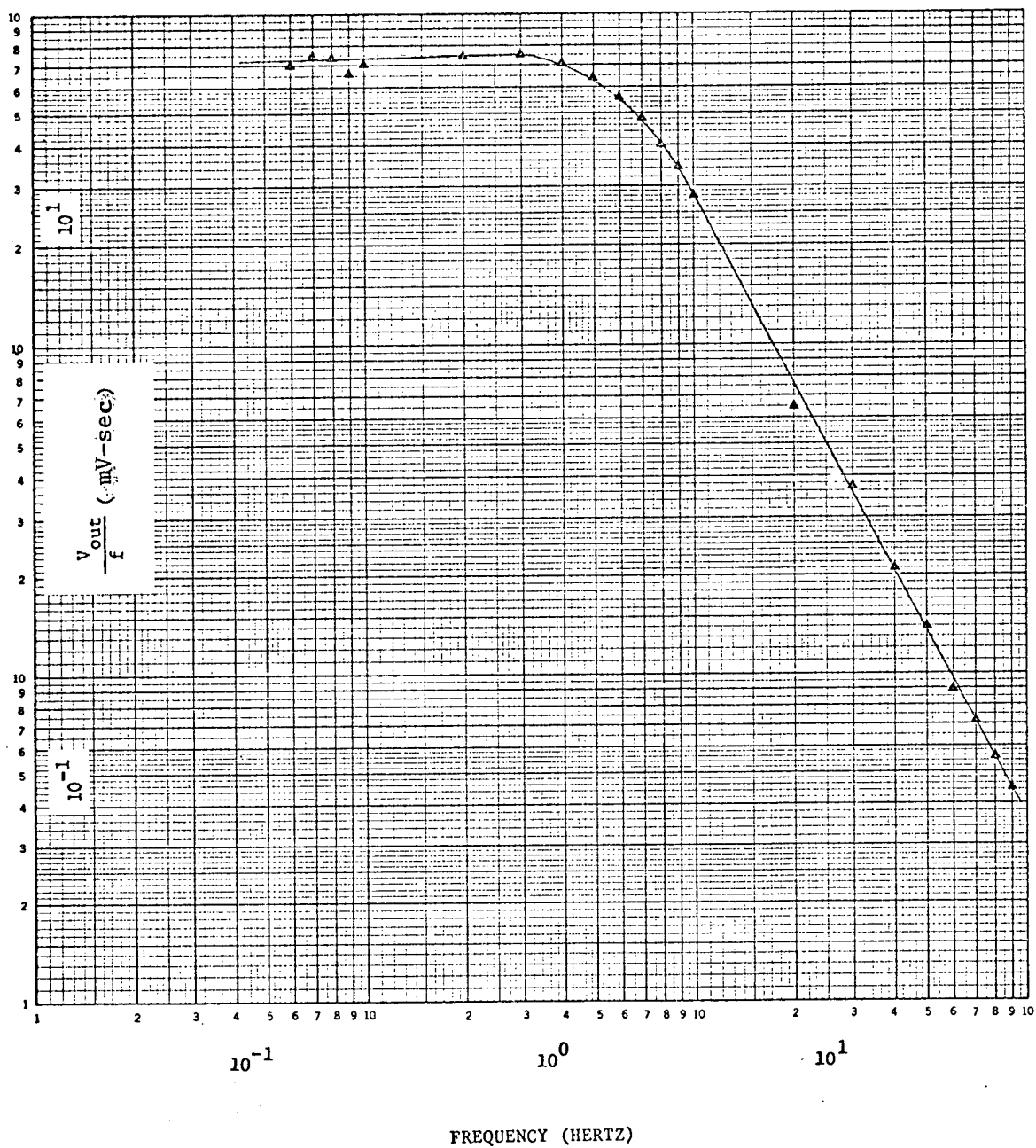


Fig. 2.3.1-2 Butterworth filter characteristics of the sensor coil system

CHAPTER III
THEORY OF THE BRIDGE METHOD

III-1 Introduction

The original idea to calibrate the induction magnetometer by using a Wheatstone bridge was conceived by Dr. R.D. Russell at the University of British Columbia. This idea stemmed from a previously successful undertaking to calibrate an electromechanical seismometer using a Maxwell bridge, Kollar and Russell (1966).

The first part of this chapter will be concerned with intuitively analyzing the Wheatstone bridge according to Norton's theorem, otherwise known as the current source model. The remainder of the chapter will present a detailed analysis according to Kirchoff's laws. The bridge system will be analyzed for three configurations. The first will be when the magnetometer is making observations and the bridge is a part of the electronics. It is hoped that the bridge can always remain a part of the magnetometer electronics so that it will not need to be wired into the system every time a calibration is made. The second configuration will be the proposed calibration procedure in which the bridge is driven by an electrical oscillator. The third will be to compare the case of observation when the bridge is not present to when it is. This last step is required in order to determine how the presence of the bridge could distort data.

III-2 An Intuitive Approach Using the Norton Equivalent

It is the intent of the development which follows to show that a rate of change of magnetic flux, $\dot{\phi}$, can be simulated in the sensor coil by driving a Wheatstone bridge with an electrical oscillator. The sensor coil will be one arm of the bridge and the equivalent circuit which will be used for it has already been given in Fig. 1-1. The Wheatstone bridge is shown in Fig. 3.2-1.

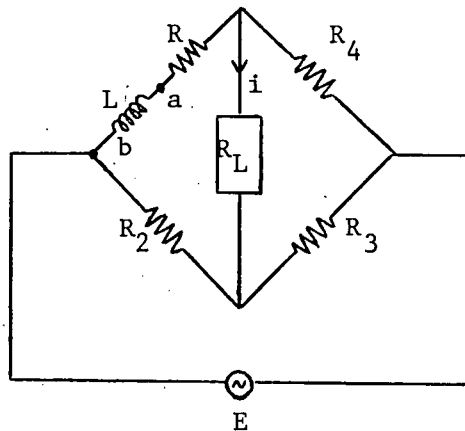


Fig. 3.2-1 The Wheatstone bridge

As the sensor is to be used for micropulsation research, frequencies of interest will be between .002 - 4 Hz, so that the capacitive reactance of Fig. 1-1 is negligible. Also, it is assumed that the amplitude of the signal from the electrical oscillator will be much larger than any signal which could be induced in the coil by a natural magnetic

event. Therefore $E \gg V$. Two further assumptions which are made concerning the magnitudes of the bridge components are:

$$\begin{aligned} R_4 &\gg R \\ R_3 &\gg R_2 \end{aligned} \quad 3.2-1$$

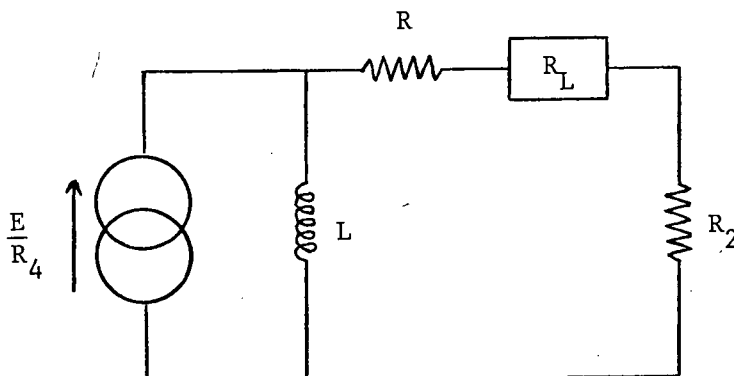
Also, the bridge is balanced at d.c.. This balancing condition is expressed as:

$$R R_3 = R_2 R_4 \quad 3.2-2$$

In order to simplify the analysis, the Norton or current source equivalent is to be found between the points a and b of Fig. 3.2-1. This is done by removing L and short circuiting the two points a and b. The current which flows between these points would be:

$$i_{a,b} = \frac{E}{R + R_4} \approx \frac{E}{R_4} \quad 3.2-3$$

Next, consider the impedance when looking in from the two terminals a and b. The impedance would be $R + R_L + R_2$ if $R_4 \gg R_L$ and $R_3 \gg R_2$. Then, the equivalent circuit which follows is:



For a coil of N turns immersed in an average magnetic flux per one turn of the coil, ϕ , the total flux through the coil is $N\phi$. Thus, the emf induced in the coil by the changing flux is:

$$E = -\frac{d}{dt}(N\phi) \quad 3.2-4$$

But, it is also true that:

$$E = -\frac{d}{dt}(Li) \quad 3.2-5$$

Applying Norton's theorem, the equivalent source current is :

$$i = \frac{N\phi}{L} \quad 3.2-6$$

Using the result of 3.2-6, the Norton equivalent of the sensor becomes:

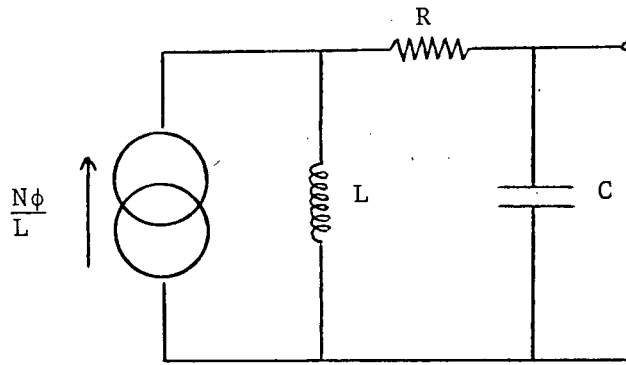


Fig. 3.2-2 Norton equivalent of the sensor coil

If the currents through the inductor in the cases of 3.2-3 and 3.2-6 are equal, then an important result exists between the amplitude of the driving voltage and the flux through the coil:

$$\frac{E}{R_4} = \frac{N\phi}{L} \quad 3.2-7$$

III-2.1 Theory at Higher Frequencies

If the Wheatstone bridge is going to be used at higher frequencies, then the capacitance of the sensor must be taken into account. To compensate for this, an inductor L_3 is added to the R_3 arm of the bridge. The bridge circuit which follows is shown in Fig. 3.2.1-1.

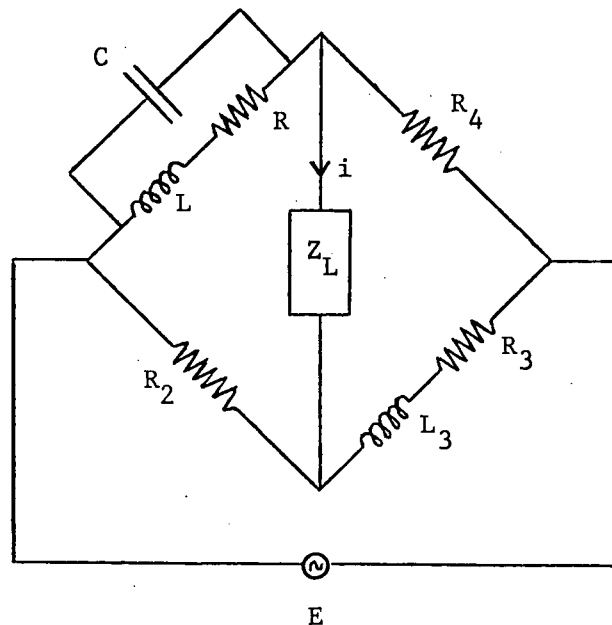


Fig. 3.2.1-1 Wheatstone bridge at higher frequencies

The Norton equivalent circuit which results from using the condition 3.2-1 is shown in the following figure.

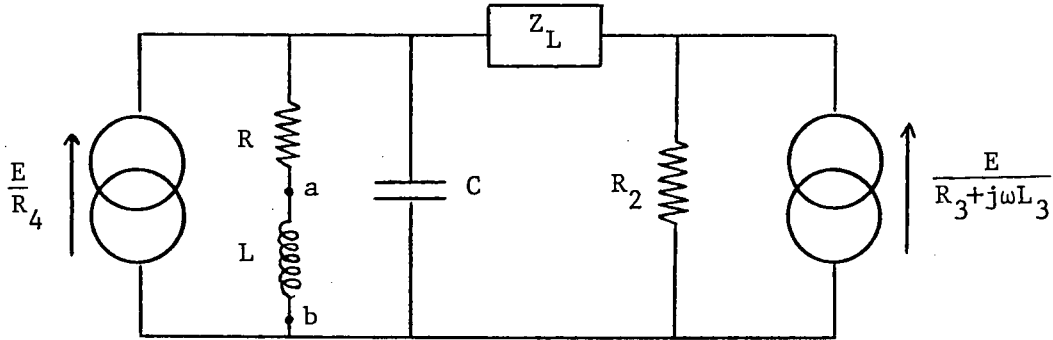


Fig. 3.2.1-2 Norton equivalent of the Wheatstone bridge

In order to arrive at a new Norton equivalent, short the two points a and b. Then calculate the current which flows through R. Currents are defined according to Fig. 3.2.1-3.

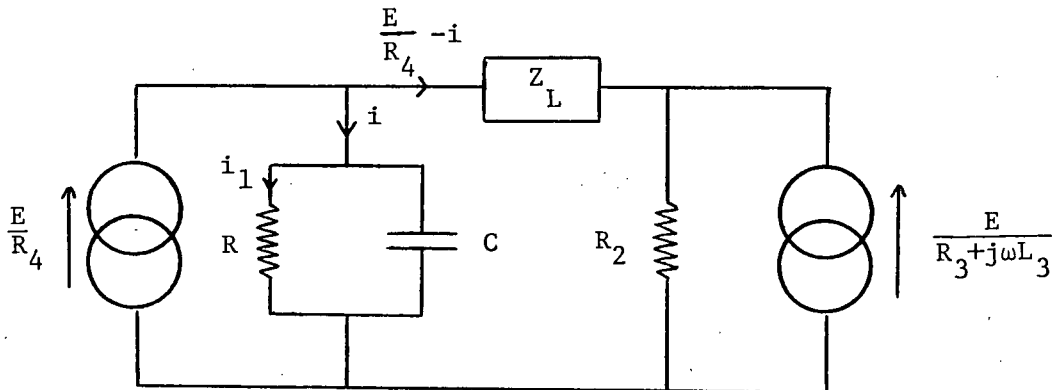


Fig. 3.2.1-3 Circuit used to derive a new Norton equivalent

Let Z_1 be the parallel composite impedance of R and C.

$$Z_1 = \frac{R}{1 + j\omega CR} \quad 3.2-8$$

Applying Kirchoff's law to the $R-Z_L-R_2$ loop, the equation which results is:

$$i \left(Z_L + R_2 + Z_1 \right) = E \left(\frac{Z_L}{R_4} + \frac{R_2}{R_4} + \frac{R_2}{R_3 + j\omega L_3} \right) \quad 3.2-9$$

Using the condition for the d.c. balanced bridge:

$$R R_3 = R_2 R_4$$

and another condition on L_3 that:

$$C R = \frac{L_3}{R_3} \quad 3.2-10$$

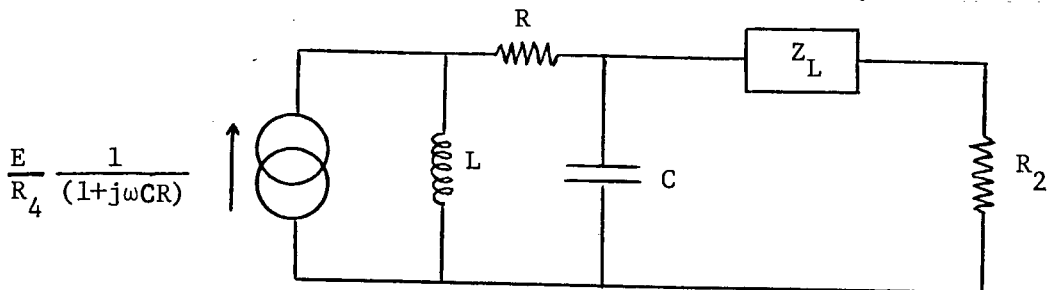
equation 3.2-9 simplifies to:

$$i = \frac{E}{R_4} \quad 3.2-11$$

Then, the current i_1 flowing through R is given by:

$$i_1 = \frac{E}{R_4} \cdot \frac{1}{(1 + j\omega C R)}$$

Therefore, the equivalent circuit becomes:



If i_1 and i of equation 3.2-6 are equal, then the result is:

$$\frac{E}{R_4} \cdot \frac{1}{(1+j\omega CR)} = \frac{N\dot{\phi}}{L} \quad 3.2-12$$

The importance of the results 3.2-12 and 3.2-7 are that they predict that a rate of change of magnetic flux, $\dot{\phi}$, can be simulated in the sensor coil by driving a Wheatstone bridge

with an electrical oscillator. In practice, it is much simpler to simulate a magnetic flux in this manner than it is to immerse the coil in a uniform calibrating field. A frequent method which is used to create an artificial field is to put the sensor coil inside a larger calibration coil. Besides being physically cumbersome so that an investigator would not want to bring a calibration coil along to the field, it costs nearly as much to build as the sensor coil. By using the Wheatstone bridge method, the calibration can be carried out at any time and with very little expense.

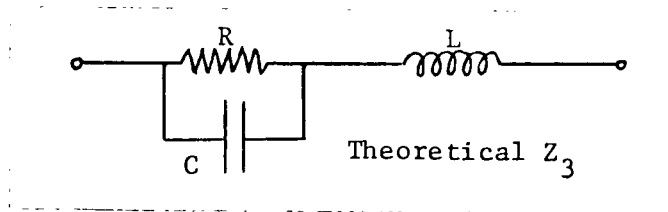
At this point, the problem of the absolute calibration is not worked out too well. The total flux $N\phi$ is related to the external field B by the relation:

$$N\phi = \int_s \vec{B} \cdot \hat{n} dA$$

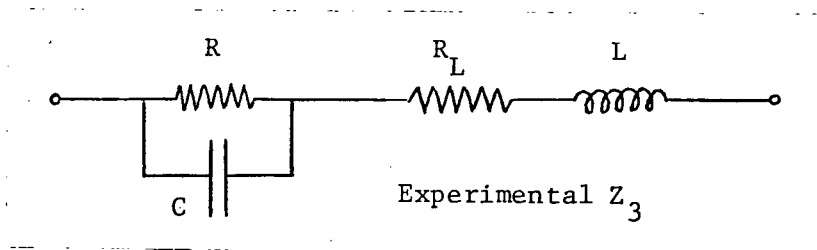
According to Dr. R.D. Russell at UBC, the calibration of sensors is reduced to finding expressions for ϕ in terms of H , and for L in terms of the coil geometry. The problem of absolute calibration will be discussed in detail in Chapter V.

III-3 Theory of the Bridge Method

A detailed circuit diagram for the bridge is shown in Fig. 3.3-1. In practice Z_0 , Z_2 and Z_4 are pure resistors. It was originally hoped that Z_3 would consist of the RLC configuration sketched below.



In this way, both an a.c. and a d.c. balance could be achieved using the bridge. Theoretically and experimentally, this configuration would work except for the fact that a large inductor, of the order of 10 Henry, could not be found which had negligible resistance. Even a resistance of 50Ω was large enough to render the a.c. balancing condition useless. A sketch of the laboratory Z_3 is shown below.



What follows is a circuit analysis of Fig. 3.3-1 which will show that this type of bridge arrangement will truly reflect the frequency response of the induction magnetometer.

Let R_1 , L_1 and C_1 be the d.c. resistance, self-inductance and capacity of the sensor. For convenience, introduce the

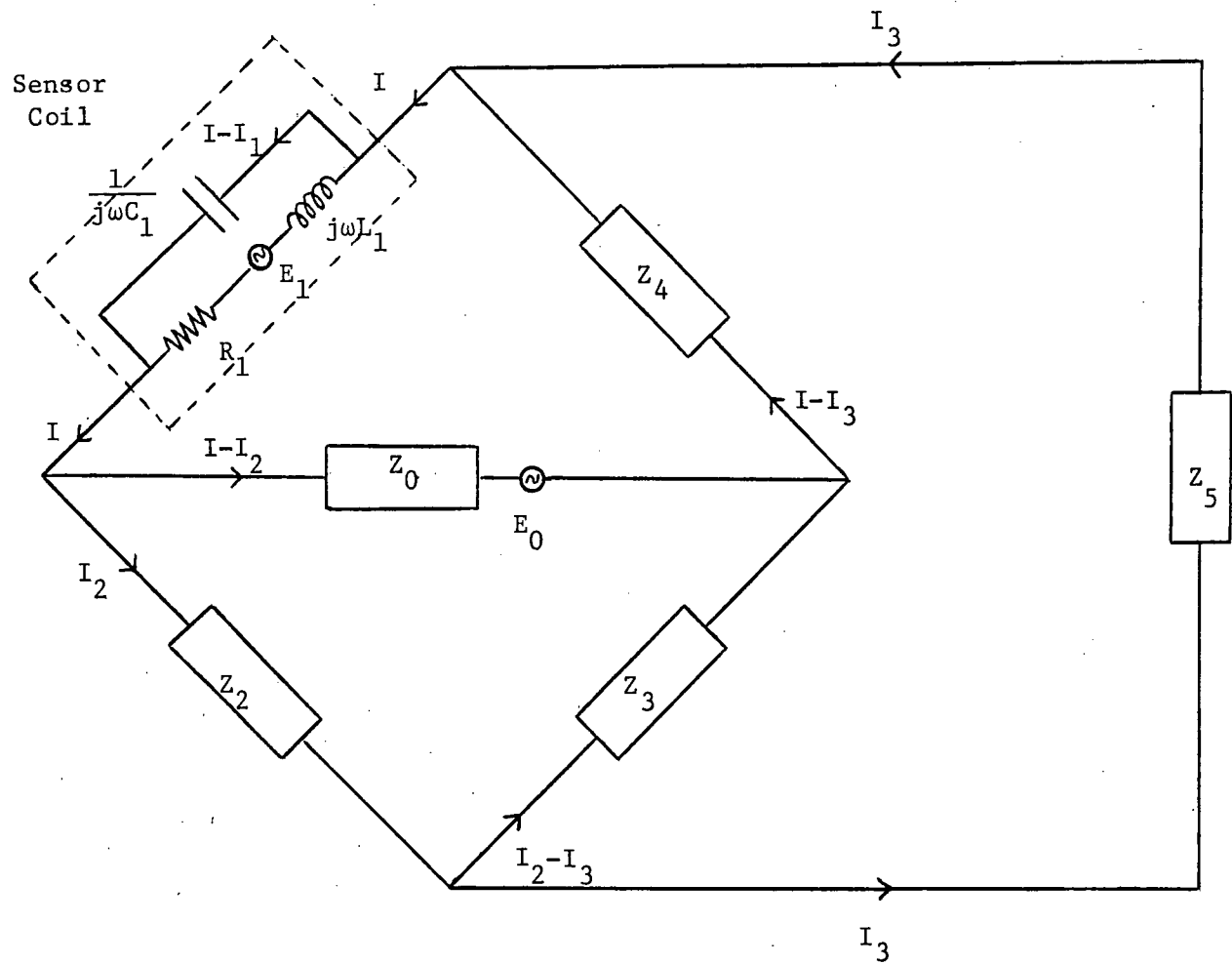


Fig. 3.3-1 The bridge circuit with parameters as they are defined for circuit analysis

quantities:

$$X_1 = R_1 + j\omega L_1 \quad 3.3-1$$

$$Y_1 = \frac{1}{j\omega C_1} \quad 3.3-2$$

$$Z_1 = \frac{X_1 Y_1}{X_1 + Y_1} \quad 3.3-3$$

E_0 will be the emf caused by the signal generator. E_1 will be the emf generated by the time variations of the magnetic field of the earth. A system of equations can now be defined by applying Kirchoff's law to current loops. The X_1 - Z_2 - Z_5 loop yields:

$$E_1 = X_1 I_1 + Z_2 I_2 + Z_5 I_3$$

The Y_1 - Z_2 - Z_5 loop yields:

$$0 = Y_1 (I - I_1) + Z_2 I_2 + Z_5 I_3$$

The Z_0 - Z_2 - Z_3 loop yields:

$$E_0 = Z_0 (I - I_2) - Z_3 (I_2 - I_3) - Z_2 I_2$$

The Z_5 - Z_4 - Z_3 loop yields:

$$0 = Z_5 I_3 - Z_4 (I - I_3) - Z_3 (I_2 - I_3)$$

These equations can be arranged, regarding I_1 , I_2 , I_3 and I as the independent variables. The corresponding matrix equation is:

$$\begin{pmatrix} E_1 \\ 0 \\ E_0 \\ 0 \end{pmatrix} = \begin{pmatrix} X_1 & Z_2 & Z_5 & 0 \\ -Y_1 & Z_2 & Z_5 & Y_1 \\ 0 & -(Z_0 + Z_2 + Z_3) & Z_3 & Z_0 \\ 0 & -Z_3 & (Z_3 + Z_4 + Z_5) & -Z_4 \end{pmatrix} \begin{pmatrix} I_1 \\ I_2 \\ I_3 \\ I \end{pmatrix} \quad 3.3-4$$

Let D be the determinant which is defined by the coefficients. It can be evaluated as follows:

$$D = -(X_1 + Y_1)D_1 - X_1 Y_1 D_2 \quad 3.3-5$$

where:

$$D_1 = Z_0 \left\{ Z_2 Z_5 + (Z_3 + Z_4)(Z_2 + Z_5) \right\} \\ + Z_4 (Z_2 Z_3 + Z_3 Z_5 + Z_5 Z_2)$$

$$D_2 = (Z_0 + Z_2 + Z_3)(Z_3 + Z_4 + Z_5) - Z_3^2$$

The current I_3 is the key to the frequency response because it flows through the load impedance Z_5 . If this method is going to properly determine the frequency response of the sensor, then it must be shown that $(I_3)_{\text{calibration}} = \text{const} * (I_3)_{\text{observation}}$. The observation condition implies that I_3 is the result of currents induced in the sensor by a fluctuating magnetic field and $E_0 = 0$. The calibration condition means that I_3 is caused by the emf of the signal generator and $E_0 \gg E_1$. Therefore, the system of simultaneous linear algebraic equations must be solved with respect to I_3 for the two cases.

III-3.1 Case of Observation

For this case, $E_1 \neq 0$ and $E_0 = 0$. The solution of the matrix equation 3.3-4 gives:

$$(I_3)_{obs} = \frac{Y_1 \{ Z_0(Z_3 + Z_4) + Z_4(Z_2 + Z_3) \}}{D} E_1 \quad 3.3.1-1$$

The natural magnetic field fluctuations may be defined in the following manner, where B is the amplitude of the field changes and S is the absolute sensitivity of the sensor coil:

$$E_1 = \pm j\omega S B e^{j\omega t} \quad 3.3.1-2$$

III-3.2 Case of Calibration

For this case, $E_0 \gg E_1$. The solution of 3.3-4 gives for $E_1 = 0$ and $E_0 \neq 0$:

$$(I_3)_{cal} = \frac{(X_1 + Y_1)(Z_1 Z_3 - Z_2 Z_4)}{D} E_0 \quad 3.3.2-1$$

The numerator of this last equation can be reduced to a simplified form by making some substitutions and approximations. First, substitute for Z_1 according to equation 3.3-3. Then:

$$(X_1 + Y_1)(Z_1 Z_3 - Z_2 Z_4) = X_1 Y_1 Z_3 - (X_1 + Y_1) Z_2 Z_4$$

Next, assume that the branches Z_2 , Z_3 and Z_4 are all pure resistors. That is $Z_2 = R_2$, $Z_3 = R_3$ and $Z_4 = R_4$. Then:

$$(X_1 + Y_1)(Z_1 Z_3 - Z_2 Z_4) = X_1 Y_1 R_3 - (X_1 + Y_1) R_2 R_4$$

Now substitute for X_1 and Y_1 according to equations 3.3-1 and 3.3-3.

$$(X_1 + Y_1)(Z_1 Z_3 - Z_2 Z_4) = \left(\frac{L_1}{C_1} R_3 - R_1 R_2 R_4 \right) - j\omega L_1 R_2 R_4 - j \frac{1}{\omega C_1} (R_1 R_3 - R_2 R_4)$$

If the bridge is balanced for the d.c. calibration signal, then the condition which is met is:

$$R_1 R_3 = R_2 R_4 \quad 3.3.2-2$$

This leads to the result:

$$(X_1 + Y_1)(Z_1 Z_3 - Z_2 Z_4) = \left(\frac{L_1}{C_1} - R_1^2 \right) R_3 - j\omega L_1 R_1 R_3$$

As $L_1 \approx 10^3 \text{H}$, $C_1 \approx 10^{-7} \text{F}$ and $R_1 \approx 10^3 \Omega$, the condition is well satisfied that:

$$\frac{L_1}{C_1} \gg R_1^2 \quad 3.3.2-3$$

The equation reduces to:

$$(X_1 + Y_1)(Z_1 Z_3 - Z_2 Z_4) = \frac{L_1}{C_1} R_3 - j\omega L_1 R_1 R_3$$

For micropulsation research, the frequency range of interest is $.002 \text{ Hz} < f < 4 \text{ Hz}$. The quotient $1/CR \approx 10^4$. Then, a final assumption can be made that:

$$\omega \ll \frac{1}{C_1 R_1} \quad 3.3.2-4$$

It should be noted that this last condition will break down at higher frequencies. Whereas it is well satisfied at the lower frequencies, below 1 Hz, at a frequency of 10 Hz, the condition is really not too well met. Substituting $C_1 = .2 \mu\text{F}$ and $R = 2\text{K}\Omega$:

$$\frac{1}{\omega C_1 R_1} \approx 40$$

Thus, the final reduction of the numerator of equation 3.3.2-1, keeping in mind that $f \leq 5 \text{ Hz}$, is:

$$(X_1 + Y_1)(Z_1 Z_3 - Z_2 Z_4) = \frac{L_1}{C_1} R_3 \quad 3.3.2-5$$

Now the ratio $(I_3)_{\text{cal}} / (I_3)_{\text{obs}}$ can be calculated using 3.3.1-1, 3.3.2-1 and 3.3.2-5:

$$\frac{(I_3)_{\text{cal}}}{(I_3)_{\text{obs}}} = \frac{j\omega L_1 R_3}{Z_0 (R_3 + R_4) + R_4 (R_2 + R_3)} \cdot \frac{E_0}{E_1}$$

Using 3.3.1-2, the final result, keeping in mind conditions 3.3.2-3 and 3.3.2-4, is:

$$\frac{(I_3)_{\text{cal}}}{(I_3)_{\text{obs}}} = \frac{\pm L_1 R_3}{Z_0 (R_3 + R_4) + R_4 (R_2 + R_3)} \cdot \frac{E_0}{SB} \quad 3.3.2-6$$

Thus, the important conclusion is that for the d.c. balanced

bridge:

$$(I_3)_{cal} \propto (I_3)_{obs} \quad 3.3.2-7$$

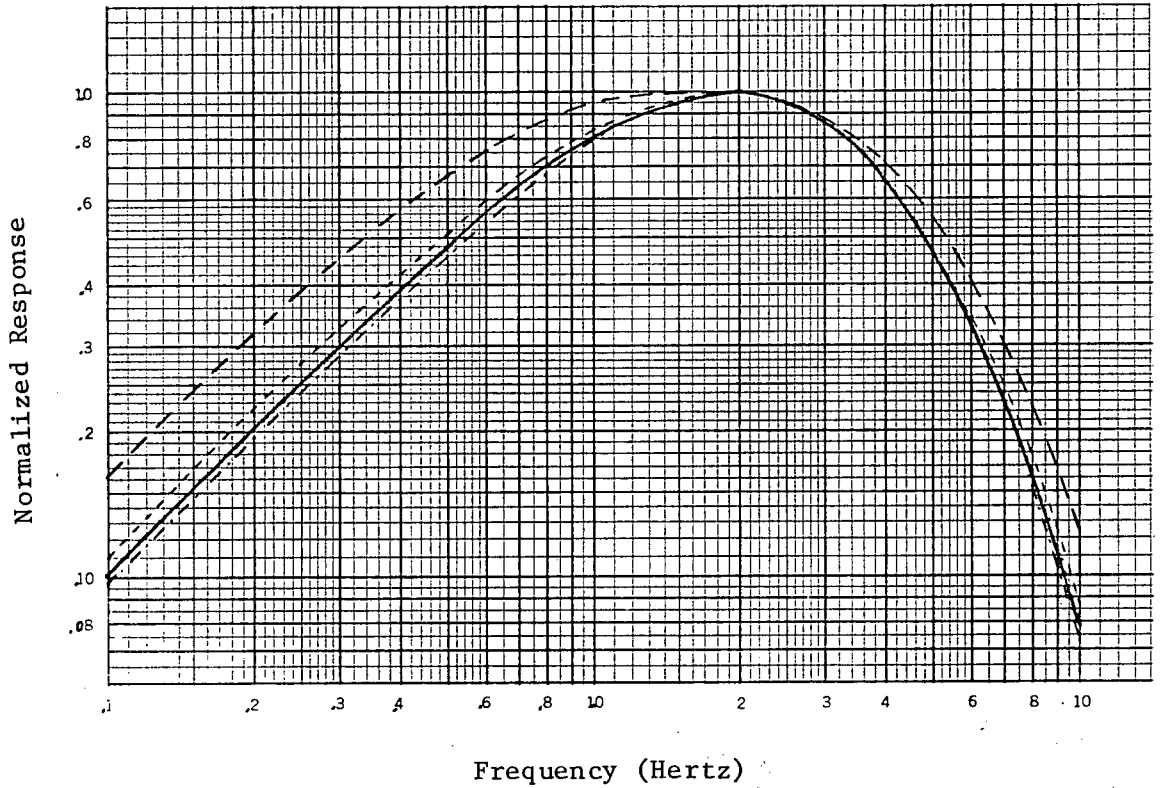
The ratio $(I_3)_{cal} / (I_3)_{obs}$ is independent of frequency. Therefore, the frequency response of $(I_3)_{cal}$ faithfully reflects that of the induction magnetometer.

III-3.3 Computer and Laboratory Results

The success of the bridge method will depend upon how well two conditions are satisfied. These conditions are:

$$\begin{aligned} R_4 &\gg R_1 \\ R_3 &\gg R_2 \end{aligned} \quad 3.3.3-1$$

If these conditions are poorly met, then the output from the bridge may differ considerably from the case when these conditions are met. A computer program was written to precisely determine how the response curve for the sensor coil would be affected by the inequality. The equation programmed was $V = (I_3)_{obs} Z_s$, where $(I_3)_{obs}$ is defined by 3.3.1-1. These results may be seen in Fig 3.3.3-1. The program was written with $R_3 = R_1$. The curve which results from $R_2 = .5R_1$, and $R_4 = 2R_1$, differs substantially from the curve when $R_2 = .02R_1$, and $R_4 = 50R_1$. There is not much difference between the curve for $R_2 = .05R_1$, and $R_4 = 20R_1$, and the curve when $R_2 = .02R_1$, and $R_4 = 50R_1$. The conclusion is that the condition $R_4 \gg R_1$ implies $R_4 \geq 20R_1$, and $R_3 \gg R_2$ implies $R_2 \leq .05R_3$.



KEY:

— —	$R_2 = 0.5R_1$	$R_4 = 2R_1$
- - - -	$R_2 = 0.1R_1$	$R_4 = 10R_1$
— — —	$R_2 = 0.05R_1$	$R_4 = 20R_1$
- - - - -	$R_2 = 0.02R_1$	$R_4 = 50R_1$

Fig. 3.3.3-1 Computer simulation to determine the effect of the conditions $R_4 \gg R_1$ and $R_3 \gg R_2$ on the response of the magnetometer system when using the bridge method

A laboratory experiment was performed to determine the frequency response of the magnetometer system using the bridge method. The circuit diagram is shown in Fig. 3.3.3-2. The bridge resistors were determined according to the conditions 3.3.2-2 and 3.3.3-1. To satisfy the condition 3.3.2-2, R_3 was made approximately equal to R_1 , $R_2 = R_1/20$ and the bridge was adjusted to zero d.c. output by the variable resistor R_4 . Also, it must be noted that the first stage of the amplifier system is a chopper amplifier (see Appendix 2) which requires a balanced input signal. This is the reason for using the inverting amplifier as part of the input signal electronics to the bridge.

The results of the laboratory test can be seen in Fig. 3.3.3-3. For convenience, the data has been normalized to the value at 2 Hz. The dots represent data points obtained in the laboratory. The smooth curve is the result of a computer analysis. The equation which was programmed is:

$$V = (I_3)_{obs} * Z_s * T(j\omega) \quad 3.3.3-2$$

$T(j\omega)$ is the transfer function for the amplifier electronics and is derived in Appendix 2. As can be seen, the agreement between theory and the laboratory is excellent.

The phase is shifted by 90° in the low frequency range. This is because the emf is induced in the coil by Faraday's law of induction which states that the emf around a stationary loop is proportional to the rate of change of flux through the loop.

$$emf = - \frac{d\phi}{dt}$$

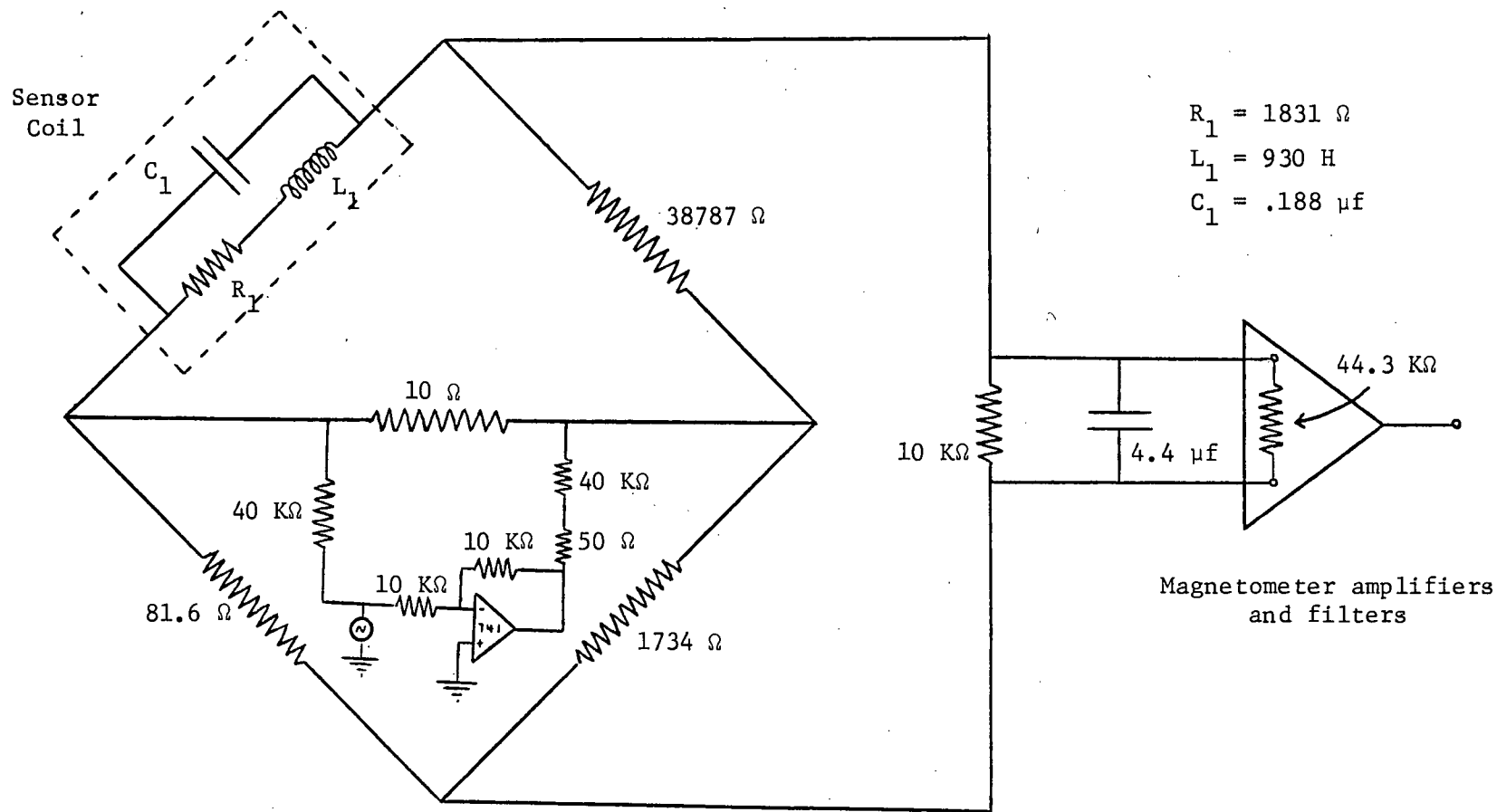


Fig. 3.3.3-2 The laboratory bridge circuit

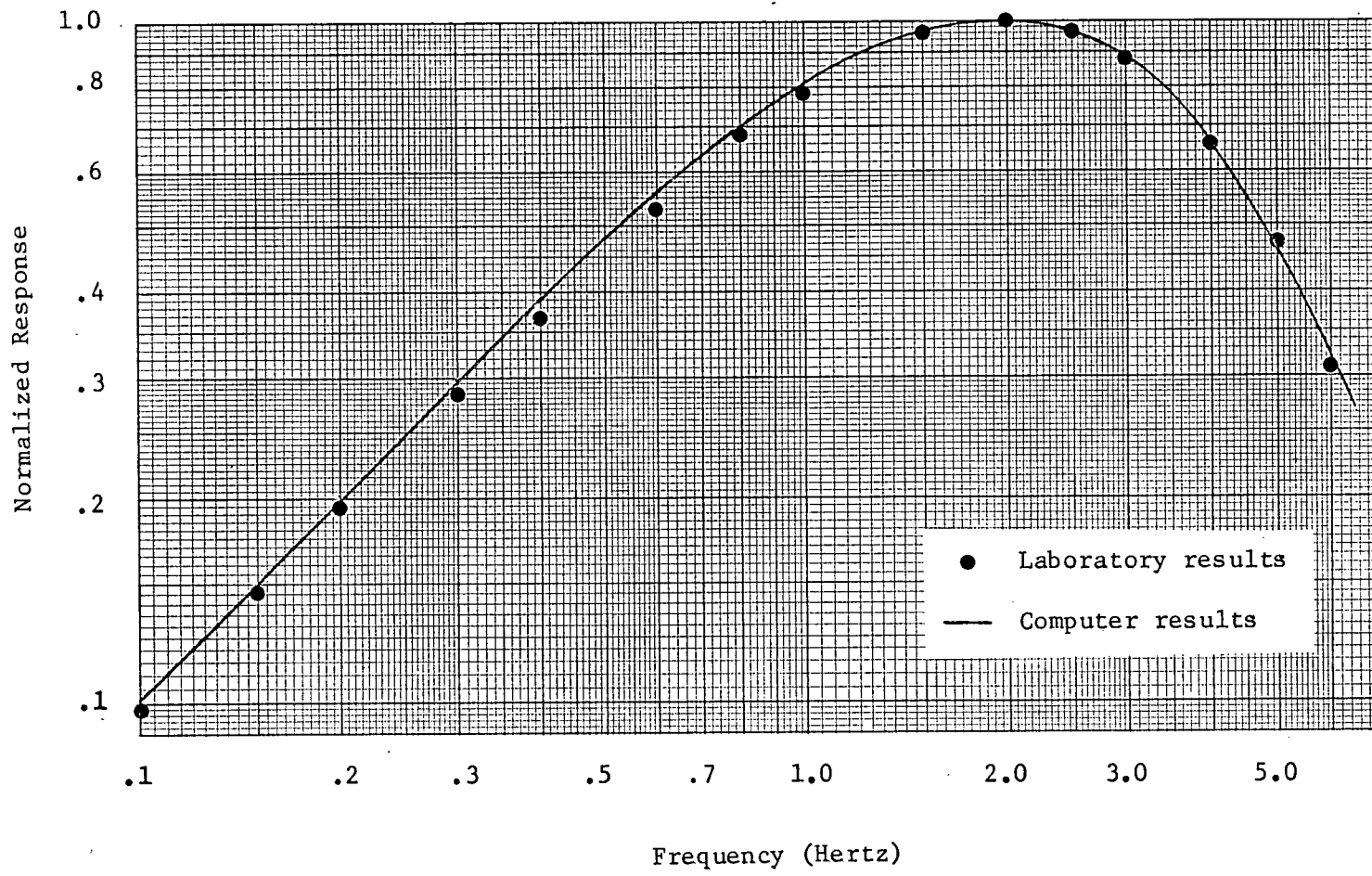


Fig. 3.3.3-3 The normalized amplitude response of the magnetometer system according to the bridge method

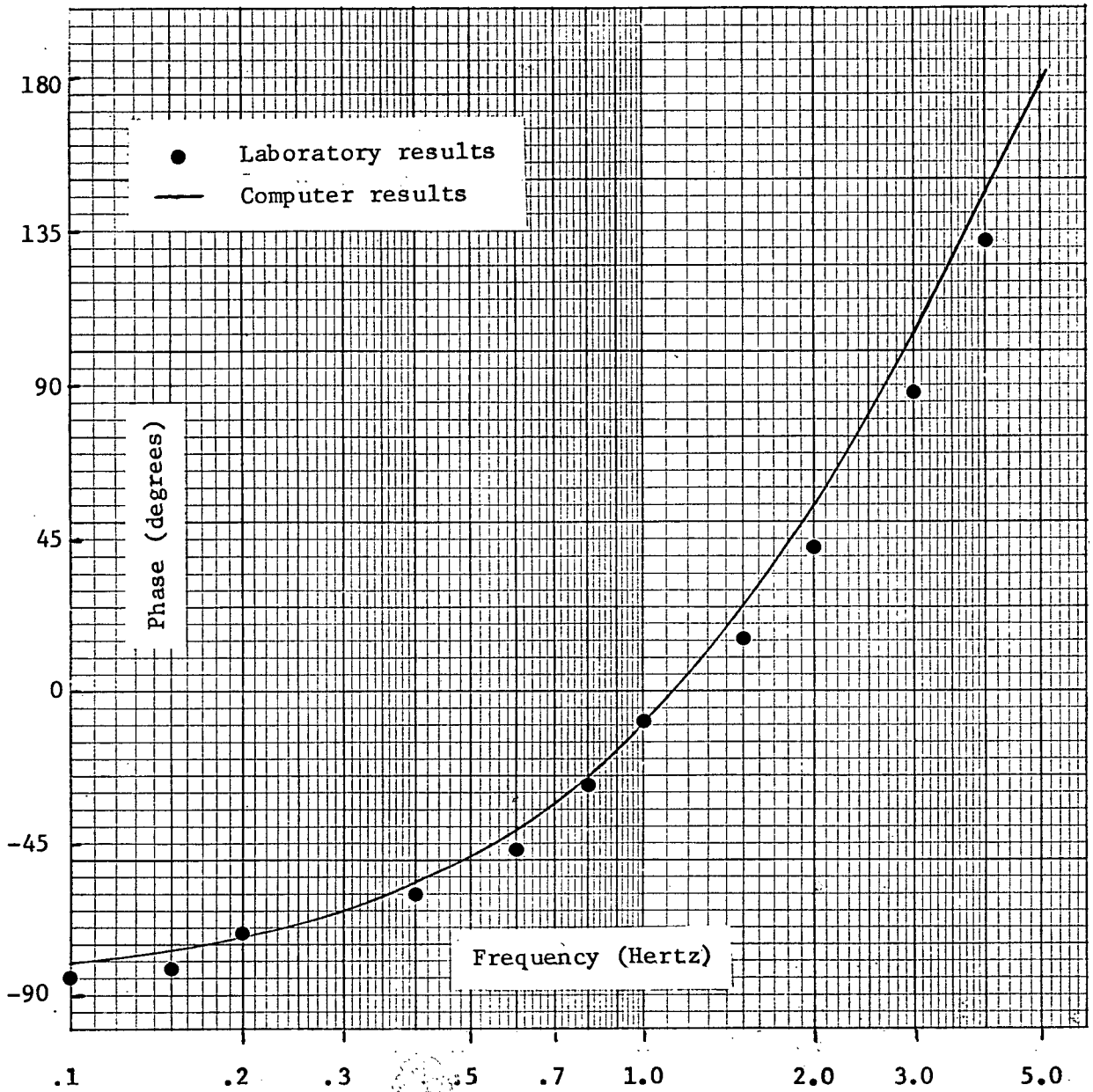


Fig. 3.3.3-4 The phase response of the magnetometer system according to the bridge method

For a field which is normal to the loop:

$$\phi = \int_s \vec{B} \cdot \vec{n} dA = BA$$

Let $B = B_0 e^{j\omega t}$. Then :

$$emf = -j\omega BA$$

Thus, it is expected that the emf will lag by 90° at the lower frequencies. At the higher frequencies, the phase will be affected by the low pass filters of the amplifier electronics, of which there are seven orders. It is no longer such a simple problem to predict what the phase response will be, as in the low frequency case.

III-4 The Case of Observation With and Without the Bridge

The voltage output as measured across Z_5 in the case of observation with the bridge can be found using eq. 3.3.3-2. It is given by $V_{obs} = (I_3)_{obs} * Z_5$.

$$V_{obs} = \frac{Y_1 \{ Z_0 (Z_3 + Z_4) + Z_4 (Z_2 + Z_3) \} Z_5}{D} E_1 \quad 3.4-1$$

It is desired that the result 3.4-1 concur with the case of observation without the bridge so that it will not be necessary to have the bridge as a permanent part of the electronics. If the sensor coil is to be operating in the field without the bridge, then a diagram representing the

input voltage to the amplifier system is shown in Fig. 3.4-1.

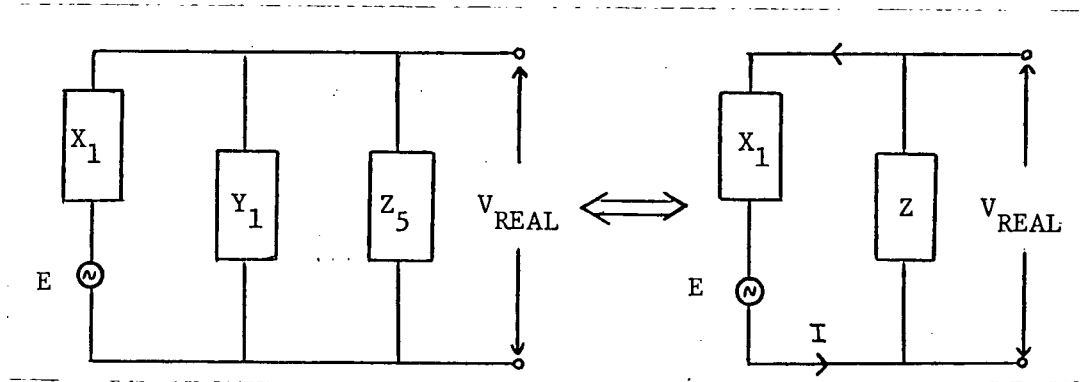


Fig. 3.4-1 Diagram of sensor coil and load impedance

X_1 and Y_1 are given by equations 3.3-1 and 3.3-2 respectively. The composite impedance of Y_1 and Z_5 is given by:

$$Z = \frac{Y_1 Z_5}{Y_1 + Z_5}$$

Then the current I is:

$$I = E / (X_1 + Z)$$

The potential drop across Z_5 is:

$$V_{\text{REAL}} = \frac{Z}{X_1 + Z} E$$

The ratio of the output voltage to the input voltage is:

$$\frac{V_{\text{REAL}}}{E} = \frac{Z}{X_1 + Z}$$

By making the substitution for Z , this last result becomes:

$$\frac{V_{\text{REAL}}}{E} = \frac{1}{X_1} \cdot \frac{Z_1 Z_5}{(Z_1 + Z_5)}$$

3.4-2

If the bridge method is going to be used for calibration purposes, then it is necessary to show that $V_{obs} \approx V_{REAL}$. The equation for V_{obs} is much more complicated than the one for V_{REAL} , but by carefully considering orders of magnitude of the quantities which are involved in each term, it can be shown that V_{obs} is essentially identical to V_{REAL} . As a starting point to evaluate these orders of magnitude, let $Z_0 = 10\Omega$, $Z_3 = R$, $Z_2 = R/20$ and $Z_4 = 20R$, where R is the resistance of the sensor coil and taken to be approximately 2000Ω . Also let $Z_5 = 10000\Omega$. By evaluating all of the terms of D according to equation 3.3-5, and retaining only the largest terms, it can be shown that:

$$D \approx Z_3 Z_4 Z_1 + Z_3 Z_4 Z_5 + Z_3 Z_1 Z_5 \quad 3.4-3$$

The error of this approximation is of the order of 6%. By evaluating the numerator of 3.4-1 with the same substitutions as were made for D , it is apparent that:

$$Z_0 (Z_3 + Z_4) + Z_4 (Z_2 + Z_3) \approx Z_3 Z_4 \quad 3.4-4$$

This approximation is of the order of 5%. With all of these reductions of terms and noting that for pure resistances $Z_3 = R_3$ and $Z_4 = R_4$, 3.4-1 becomes:

$$V_{obs} \approx \frac{Y_1 R_4 Z_5}{(X_1 + Y_1) \{ R_4 (Z_1 + Z_2) + Z_1 Z_5 \}} E_1 \quad 3.4-5$$

Upon rearranging terms:

$$V_{obs} \approx \frac{Z_1 Z_5}{X_1 (Z_1 + Z_5)} \cdot \frac{1}{1 + \frac{1}{R_u} \left(\frac{Z_1 Z_5}{Z_1 + Z_5} \right)} E_1 \quad 3.4-6$$

If R_u can be made large enough, then the radical in the denominator containing R_u becomes small and V_{obs} reduces to:

$$V_{obs} \approx \frac{1}{X_1} \cdot \frac{Z_1 Z_5}{(Z_1 + Z_5)} E_1 \quad 3.4-7$$

This is identical to 3.4-2. It must be noted that R_u of 3.4-6 cannot be increased to a very high value without reconsidering the approximations of 3.4-3 and 3.4-4. If R_u is to be made larger than 20 times the sensor coil resistance, then it is imperative that Z_2 and Z_0 be small, certainly less than 100Ω and preferably of the order of 10Ω . Otherwise, the approximations leading to 3.4-7 will no longer be valid and the voltage output as measured across Z_5 in the case of observation with and without the bridge will no longer be comparable.

The physical significance of 3.4-6 is interesting in itself. What it means is that the bridge circuit of Fig. 3.3-1 with $E_0=0$ effectively reduces to the following:

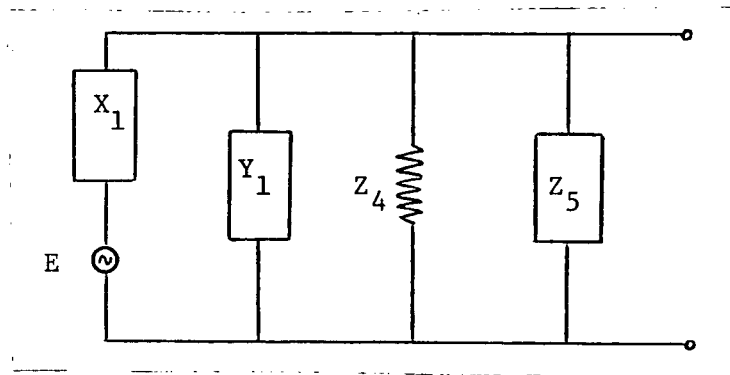


Fig. 3.4-2 The essential elements of the bridge circuit

The effect of the term containing R_q has been observed from computer simulations. The results of the computer analysis can be seen in Fig. 3.4-3. Equation 3.3.3-1 was programmed with and without the R_q term as given by 3.4-6. The same values of bridge components were used as shown in Fig. 3.3.3-2. It can be seen that the effect of Z_q is to cause a small separation between the two curves with the maximum separation occurring at 2 Hz.

By comparing Fig. 3.4-1 and 3.4-2, the final conclusion reached is that $V_{obs} \approx V_{REAL}$ only if the effect of Z_q can be reduced by making it a high value. This infers that the comparison of observations between two systems, one with the bridge as a permanent part of the electronics and another without the bridge, may have a slight discrepancy which can be attributed primarily to Z_q acting as a parallel load across the output of the sensor system.

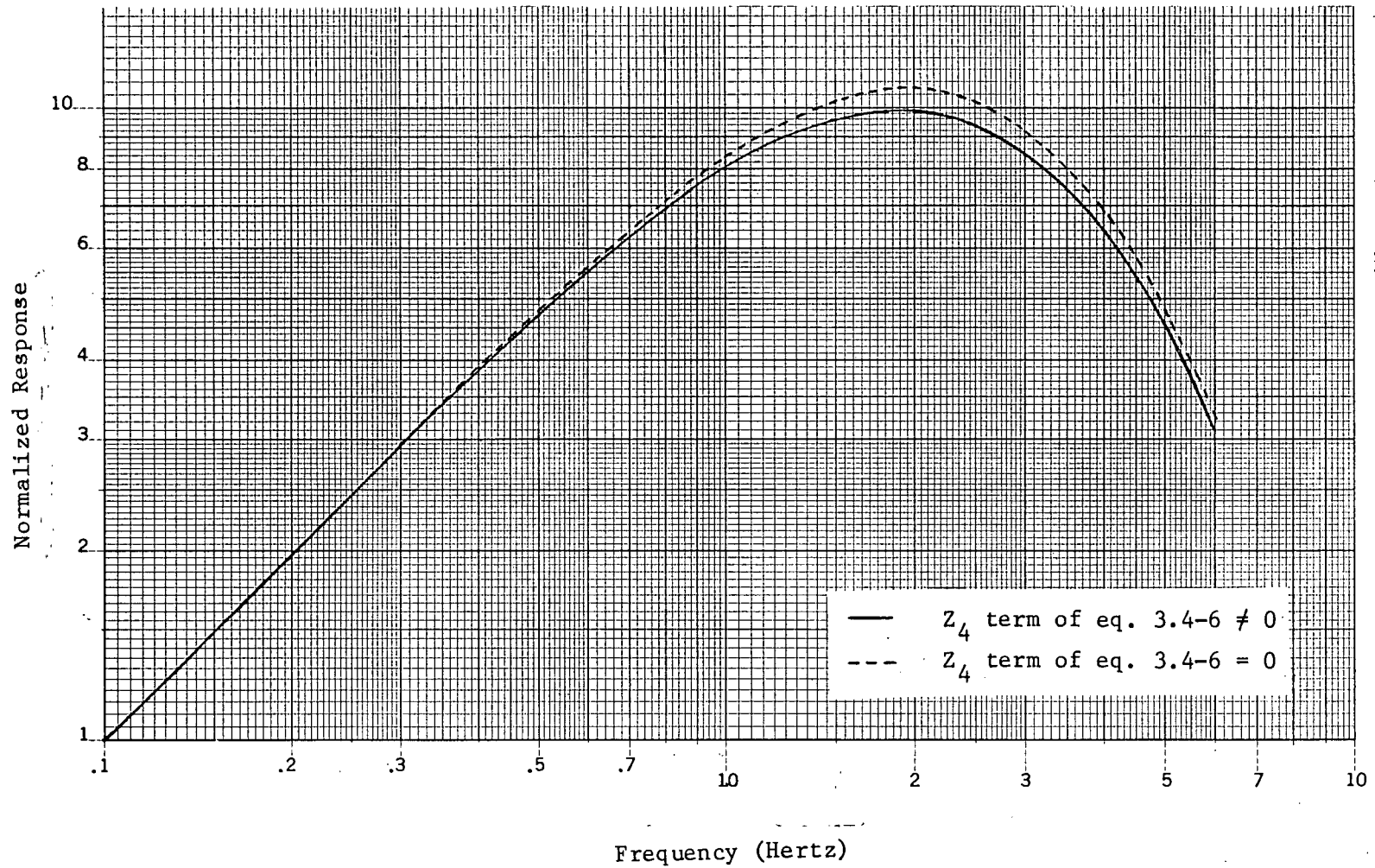


Fig. 3.4-3 The effect of the resistance R_4 on the frequency response as obtained from the Bridge method

CHAPTER IVTHEORY OF THE SECONDARY COIL METHODIV-1 Introduction

When using this method to determine the frequency response of the magnetometer system, a time varying magnetic field is created by a secondary coil. The secondary coil is aligned coaxially with the sensor coil and at the center of the coils is a Mu-metal core. The field is detected by the sensor coil. It is the purpose of the derivations which follow to show that the frequency response can be accurately determined using this approach. As in the case of the bridge method, the input voltage to the amplifier system will be derived when the system is being calibrated and also when it is in its normal observational mode. Finally, a comparison will be made between the frequency response which is obtained from the secondary coil method to the one obtained from the bridge method.

IV-2 Theory of Operation

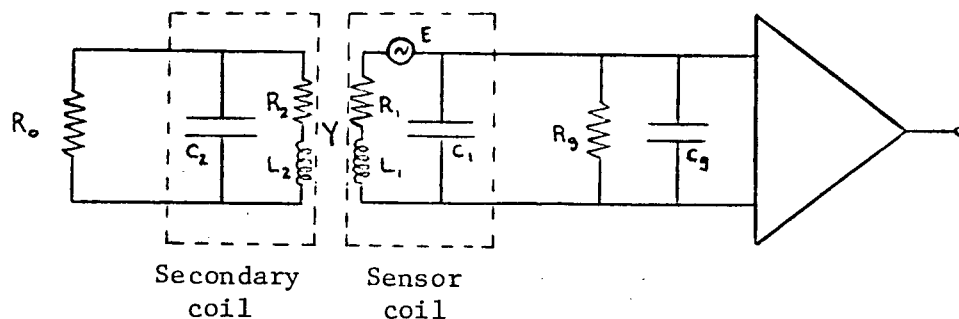


Fig. 4.2-1 The secondary coil method at the time of operation

The circuit which is representative of the magnetometer system when it is in the observational mode is depicted in Fig. 4.2-1. The parameters C_2 , R_2 and L_2 are the secondary coil constants. Y is defined as:

$$Y = j\omega M \quad 4.2-1$$

where M is the mutual inductance between the two coils. R_o is the load on the secondary coil that is adjusted to remain constant when the signal generator is added for calibration purposes (see Figs. 4.2-1 and 4.3-1). The sensor coil constants are R_1 , L_1 and C_1 . Because of the geometry of the two coils and the fact that they have a μ -metal core in common, there is a possibility that the response of the sensor coil in the observational mode could be distorted by mutual inductance between itself and the secondary coil. It is the purpose of this section to explore this problem in detail.

Let

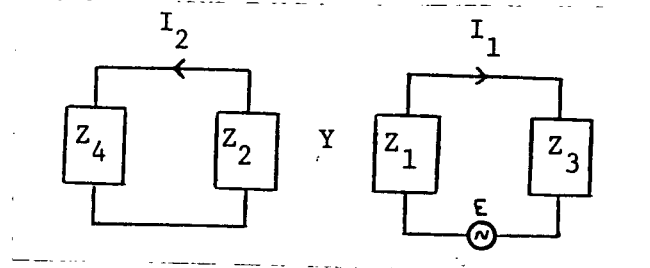
$$Z_1 = R_1 + j\omega L_1 \quad 4.2-2$$

$$Z_2 = R_2 + j\omega L_2 \quad 4.2-3$$

$$\frac{1}{Z_3} = j\omega(C_1 + C_2) + \frac{1}{R_3} \quad 4.2-4$$

$$\frac{1}{Z_4} = j\omega C_2 + \frac{1}{R_0} \quad 4.2-5$$

Then, the equivalent circuit at the time of operation for observation becomes:



Applying Kirchoff's theorem, the two circuit equations are:

$$(Z_1 + Z_3) I_1 = E - Y I_2$$

$$(Z_2 + Z_4) I_2 = -Y I_1$$

The solution for I_1 is:

$$I_1 = \frac{(Z_2 + Z_4)}{(Z_1 + Z_3)(Z_2 + Z_4) - Y^2} E \quad 4.2-6$$

The input voltage to the amplifier is $V_3 = I_1 Z_3$. In order to make I_1 independent of any effects from the secondary coil, the following condition must be satisfied:

$$|(Z_1 + Z_3)(Z_2 + Z_4)| \gg |Y|^2 \quad 4.2-7$$

An upper limit to the magnitude of Y can be found by putting a bound on M . If the self inductance of the two coils are known and it is assumed that all the magnetic lines of force set up by the first coil cut all the turns of the second coil, then

the mutual inductance M is given by:

$$M = \sqrt{L_1 L_2} \quad 4.2-8$$

It is not certain what percentage of magnetic lines set up by one coil will cut the turns of the other coil, so it is safer to make this last equation into an inequality.

$$M \leq \sqrt{L_1 L_2} \quad 4.2-9$$

Then, it is of interest to show that:

$$\frac{(Z_1 + Z_3)(Z_2 + Z_4)}{\omega^2 L_1 L_2} \gg 1$$

For the coils used, $L_1 \approx 1000$ H and $L_2 \approx .01$ H. Also, $C_g = 4.5 \mu\text{f}$ and $R_g = 7.5$ K Ω . The coil constants are given in Table I-1. A reasonable worst case result, which would be at the highest possible frequency that one might expect to observe micropulsations, would be at 10 Hz. Substituting these numbers into the last inequality:

$$\frac{(Z_1 + Z_3)(Z_2 + Z_4)}{\omega^2 L_1 L_2} = \frac{720,000}{900} = 800$$

Thus, the condition 4.2-7 is easily satisfied. The final result for the input voltage to the amplifier system is given by $V_{\text{obs}} = Z_3 I_3$:

$$V_{\text{obs}} = \frac{Z_3}{Z_1 + Z_3} E \quad 4.2-10$$

The conclusion is that the induction magnetometer at the time of operation for observation is unaffected by the presence of the secondary coil.

IV-3 Theory of Calibration

In this section the calibration procedure will be discussed. A time varying magnetic field will be induced into the sensor coil by a signal from the secondary coil. It will be assumed that this signal is much larger in magnitude than any natural magnetic fluctuations so that E as defined in Fig. 4.2-1 can be considered negligible. A circuit diagram for the calibration is shown in Fig. 4.3-1.

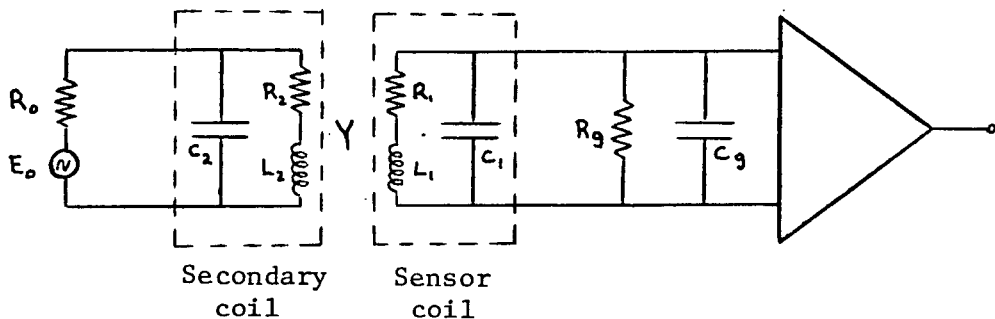


Fig. 4.3-1 The secondary coil method at the time of calibration.

In order to simplify the picture for algebraic calculations, the following substitutions will be made:

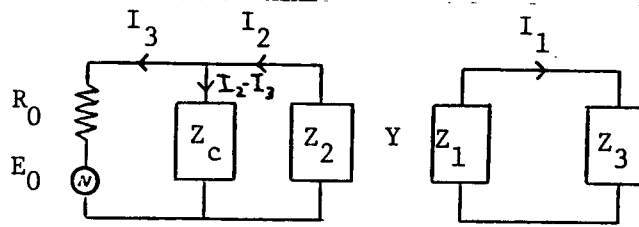
$$Z_1 = R_1 + j\omega L_1$$

$$Z_2 = R_2 + j\omega L_2$$

$$\frac{1}{Z_3} = j\omega(C_1 + C_g) + \frac{1}{R_g}$$

$$Z_c = \frac{1}{j\omega C_2}$$

The equivalent circuit diagram at the time of calibration becomes:



There are three loop equations which result.

$$\begin{aligned}(Z_1 + Z_3)I_1 &= -YI_2 \\ Z_2I_2 + Z_c(I_2 - I_3) &= -YI_1 \\ Z_c(I_2 - I_3) - I_3R_0 &= -E_0\end{aligned}$$

Solving this system of equations for I_1 :

$$I_1 = - \frac{Z_c}{(Z_c + R_0)} \frac{Y}{(Z_1 + Z_3)(Z_2 + Z_4) - Y^2} E_0$$

$$\text{where } Z_4 = \frac{R_0 Z_c}{R_0 + Z_c}$$

$Z_c/(Z_c + R_0) = 1/(1 + j\omega C_2 R_0)$ is approximately equal to 1 if

$$|\omega C_2 R_0| \ll 1^*$$

The laboratory value for R_0 is $6 \text{ K}\Omega$. C_2 includes the capacitance of the secondary coil and that of the cable connecting the secondary coil to the signal generator. The cable is normally long, frequently 100 meters or more. The capacitance of the cable is of the order of 10 nf. A typical cable capacitance is 50 pf/ft. Then, the total capacitance for 100m is approximately 15 nf. The capacitance of the secondary

* This is not a necessary restriction, but a convenience.

coil should be much smaller than this. Therefore, at 10 Hz, $\omega C_2 R_0 \approx (20\pi) (6 \text{ K}) (1.5 \times 10^{-8}) = 5.65 \times 10^{-3} \ll 1$. It has already been shown that:

$$|(Z_1 + Z_3)(Z_2 + Z_4)| \gg Y^2$$

Therefore, the simplified result for the current I_1 is:

$$I_1 = - \frac{Y}{(Z_1 + Z_3)(Z_2 + Z_4)} E_0$$

The resulting voltage drop across the input to the amplifier system when the magnetometer is being calibrated is $V_{cal} = I_1 Z_3$:

$$V_{cal} = - \frac{Y Z_3}{(Z_1 + Z_3)(Z_2 + Z_4)} E_0 \quad 4.3-1$$

The ratio V_{obs} / V_{cal} can now be found using equations 4.2-10 and 4.3-1.

$$\frac{V_{obs}}{V_{cal}} = - \frac{Z_2 + Z_4}{Y} \cdot \frac{E}{E_0} \quad 4.3-2$$

The emf induced in the sensor coil by natural magnetic field fluctuations can be described by:

$$E = \frac{S}{2\pi} \omega B e^{j(\omega t - \frac{\pi}{2})} \quad 4.3-3$$

where S is the sensitivity coefficient and B is the amplitude of the oscillating magnetic field. Substituting 4.3-3 and 4.2-1 into 4.3-2, the result is:

$$\frac{V_{obs}}{V_{cal}} = \frac{1}{2\pi} \frac{SB}{ME_s} (Z_2 + Z_4) e^{j\omega t} \quad 4.3-4$$

The final observation to make is that the a.c. signal from the signal generator is given by:

$$E_o = E_s e^{j\omega t}$$

Then :

$$\frac{V_{obs}}{V_{cal}} = \frac{1}{2\pi} \frac{SB}{ME_s} (Z_2 + Z_4) \quad 4.3-5$$

$$\frac{V_{obs}}{V_{cal}} = \frac{1}{2\pi} \frac{SB}{ME_s} (R_2 + j\omega L_2 + R_o) \quad 4.3-6$$

As shown previously, $\omega C_2 R_o \ll 1$ and this implies that $Z_4 = R_o$. In order to make 4.3-6 independent of frequency, the following condition must be met:

$$(R_2 + R_o) \gg \omega L_2 \quad 4.3-7$$

Again, the worst case would be at the high frequency end, at 10 Hz. Substitute the values $R_2 = 11 \Omega$, $R_o = 6 \text{ K}\Omega$ and $L = .01 \text{ H}$.

Then :

$$\frac{\omega L_2}{R_2 + R_o} \approx \frac{(20\pi)(.01)}{6 \times 10^3} \approx 10^{-4} \ll 1$$

The condition 4.3-7 is easily satisfied. The final result is:

$$\frac{V_{obs}}{V_{cal}} = \frac{1}{2\pi} \cdot \frac{SB}{ME_s} (R_2 + R_o) \quad 4.3-8$$

Thus, it is seen that the voltage output at the time of calibration is directly proportional to the output at the time of observation. It is expected that this method of calibration will correctly produce the frequency response of the magnetometer system.

The laboratory circuit diagram for the secondary coil method is shown in Fig. 4.3-2.

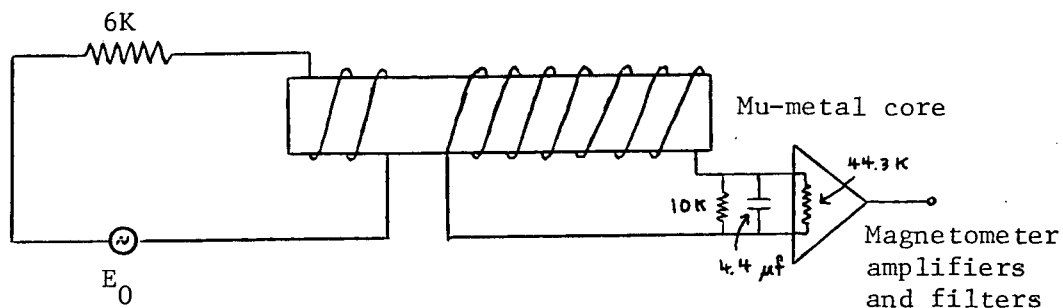


Fig. 4.3-2 The secondary coil method in the laboratory

The results from the laboratory analysis can be seen in Fig. 4.3-3 which shows the normalized frequency response and in Fig. 4.3-4 which shows the phase response. In both cases, the laboratory data is plotted as squares and the smooth curve represents the results of a computer analysis. The equation programmed is :

$$V = \frac{1}{X_1} \cdot \frac{Z_1 Z_5}{(Z_1 + Z_5)} T(j\omega) \quad 4.3-9$$

where X_1 and Z_1 are defined by 3.3-1 and 3.3-3 and :

$$Z_s = R_{load} + \frac{1}{j\omega C_{load}} = \frac{(10K)(44.3K)}{(54.3K)} + \frac{1}{j\omega(4.4\mu f)}$$

This follows from eq. 3.4-7 and from the derivation of the amplifier system transfer function given in the appendix. The agreement is ~~excellent~~ between the data obtained experimentally and the results predicted from the computer analysis.

A plot with laboratory data can now be made which is analogous to the computer plot of Fig. 3.4-3. This can be done simply by comparing the laboratory results obtained from the bridge method and the secondary coil method. On the same graph appears the laboratory data of Fig. 3.3.3-3 and Fig. 4.3-3. This is shown in Fig. 4.3-5. The agreement between the computer analysis of Fig. 3.4-3 and the laboratory analysis of Fig. 4.3-5 is excellent.

A comparison of the results of the phase analysis from the bridge method and the secondary coil method is shown in Fig. 4.3-6. The agreement between the two methods is quite good.

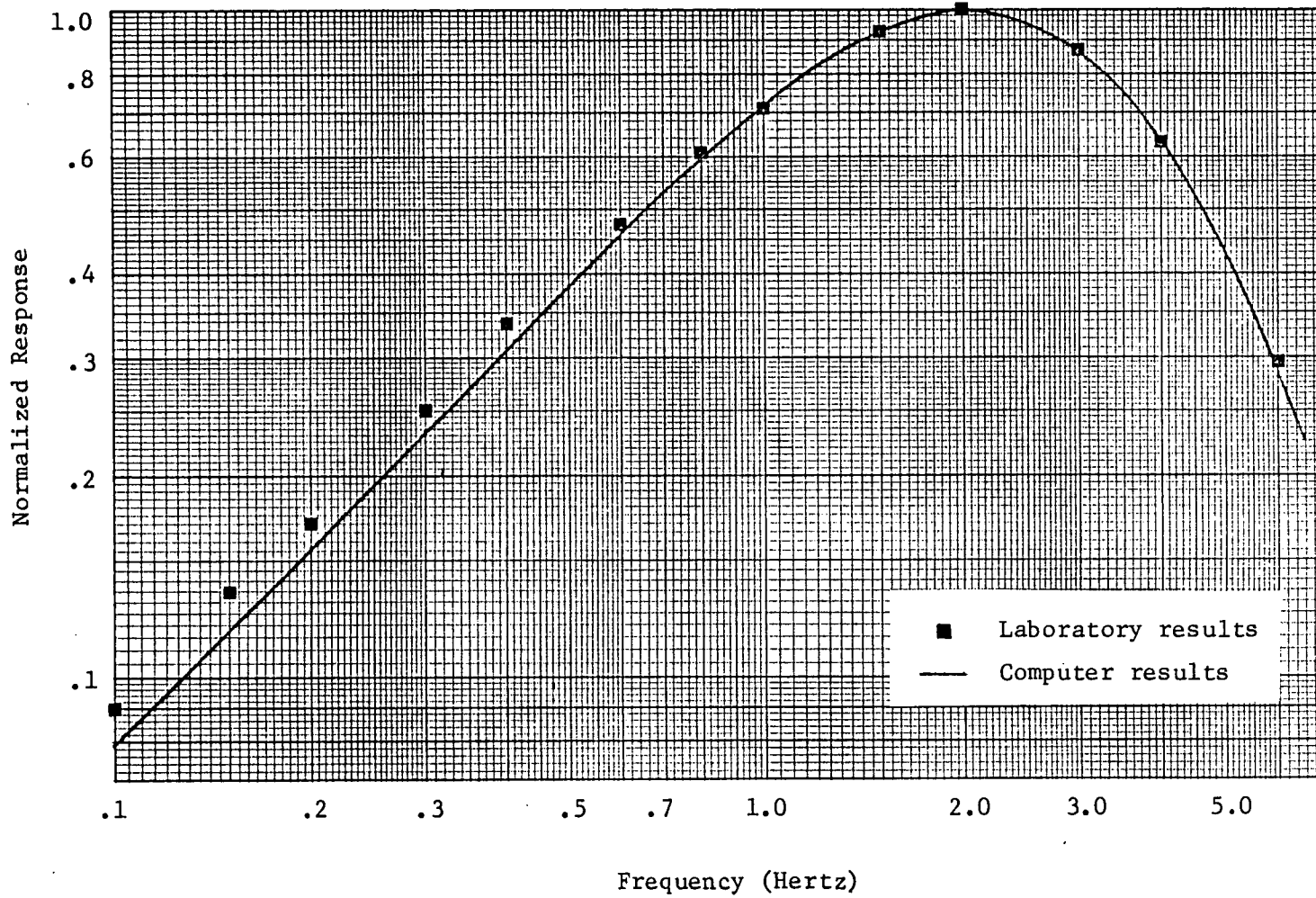


Fig. 4.3-3 The normalized amplitude response of the magnetometer system according to the secondary coil method

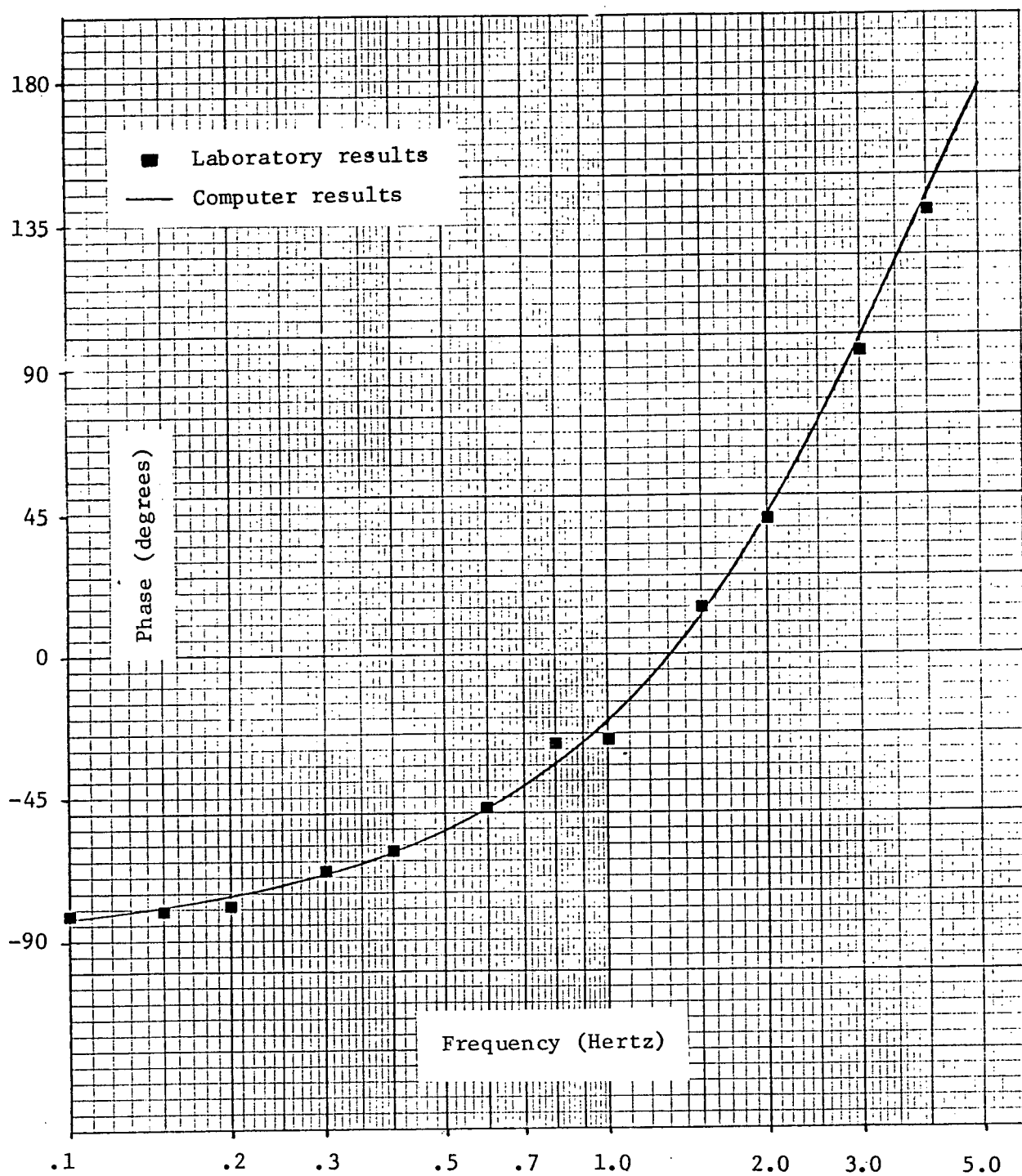


Fig. 4.3-4 The phase response of the magnetometer system according to the secondary coil method

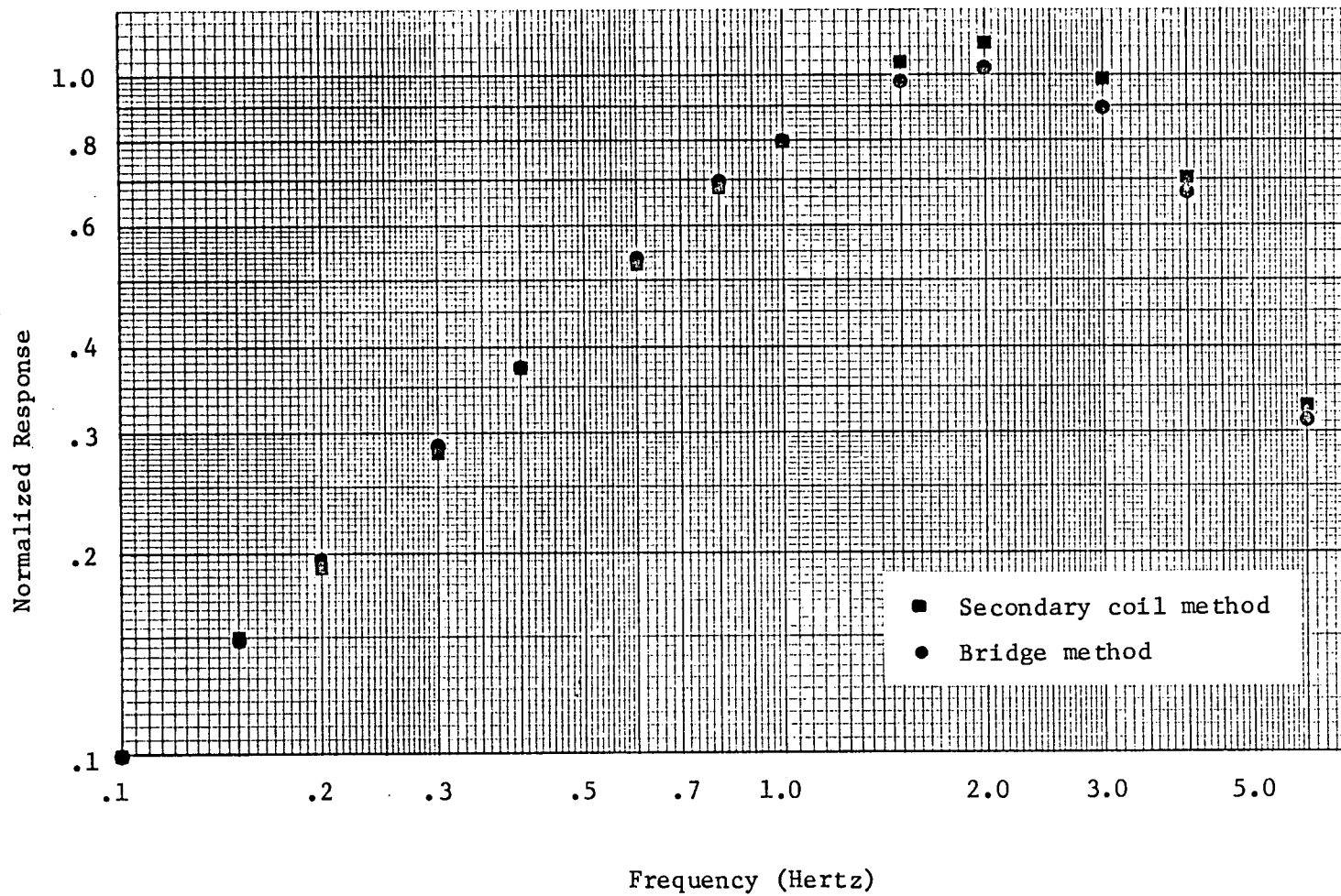


Fig. 4.3-5 A comparison of the frequency response curves obtained in the laboratory from the secondary coil method and the bridge method (see Fig. 3.4-3 and discussion on page 50 about the separation between the curves).

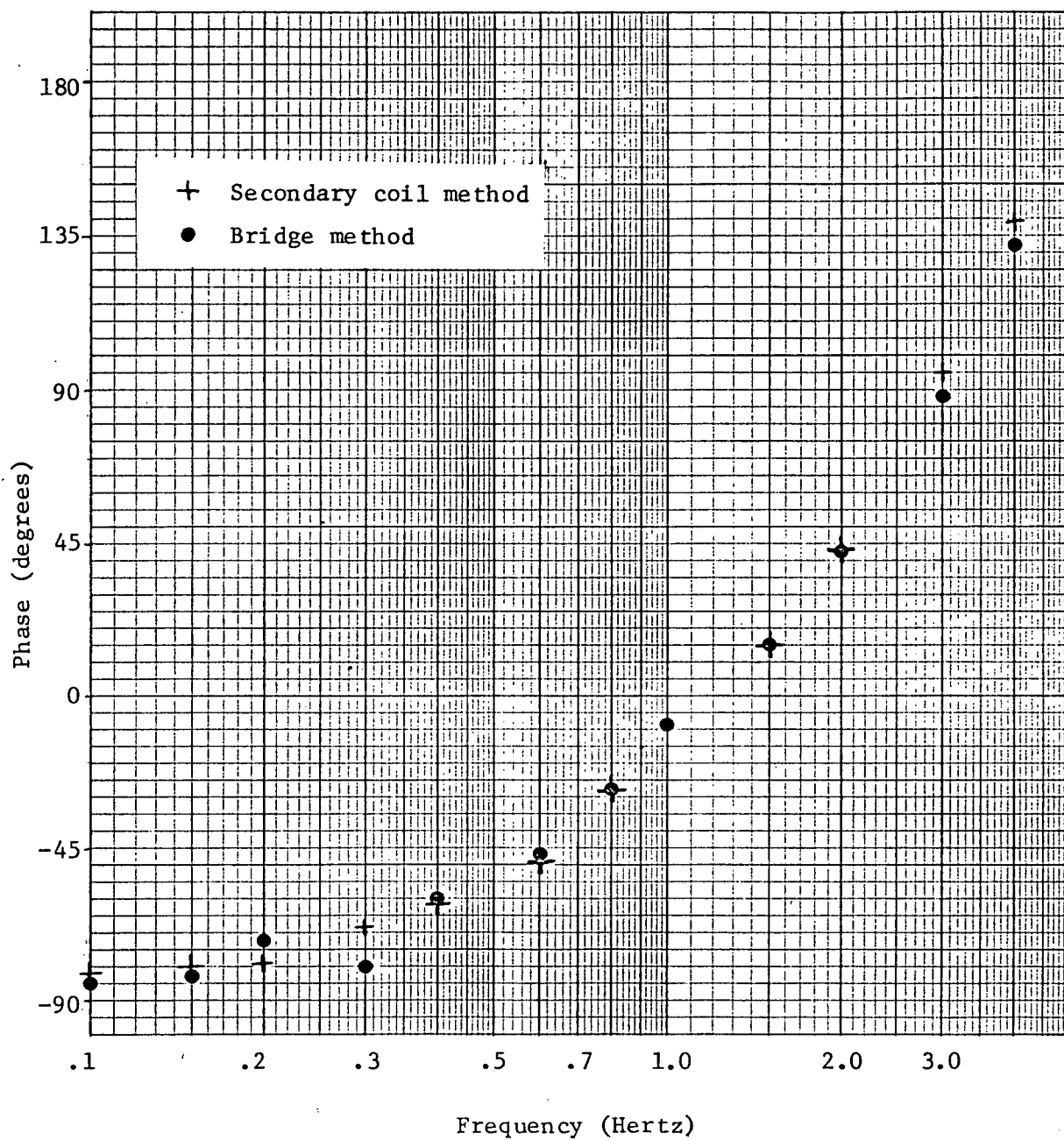


Fig. 4.3-6 A comparison of the phase response curves obtained in the laboratory from the secondary coil method and the bridge method

CHAPTER V

THE ABSOLUTE CALIBRATION

V-1 A Laboratory Approach

Now that the relative sensitivity of the Mu-metal core system is well known, it is necessary to determine the absolute sensitivity. Conceptually, the simplest way to do this would be to put the sensor coil in a known, uniform, sinusoidally varying magnetic field and record the response of the system. In practice, it is not easy to create an artificial field which would be uniform over a volume large enough to accommodate a three foot long sensor coil. A logical solution is to use the earth's natural magnetic field when a sinusoidal micropulsation event is occurring. An air core coil magnetometer system is used to precisely determine the absolute amplitude of the micropulsation event. The air core coil and the Mu-metal core coil are located about 100 yards apart and it is assumed that the natural event is uniform over this distance. The response of the Mu-metal core system can then be compared to that of the air core system, thus determining the absolute sensitivity of the Mu-metal core magnetometer. It is necessary to do this at only one frequency as the relative frequency response is already known and linearity is assumed.

The flux, $\bar{\Phi}$, through a circular coil is : $\bar{\Phi} = AB$ 5.1-1
 where $A = \pi R^2 * N$ is the average cross-sectional area times the

number of turns and B is the magnetic field strength. The electromotive force induced by the changing flux is:

$$V_{emf} = \frac{d\Phi}{dt} = A \frac{dB}{dt} \quad 5.1-2$$

The output voltage from the amplifier system, with a d.c. gain G and an input impedance R_i , which would be observed is given by 5.1-3. $H(f)$ is the transfer function normalized to the d.c. value and R is the d.c. resistance of the coil.

$$V_{out} = V_{emf} \times G \times H(f) \times \frac{R_i}{R_i + R} \quad 5.1-3$$

It is convenient for micropulsation research to express electromotive force in micro-volts and magnetic field strength in milli-gauss. This leads to the following two equations where V_{emf} is in volts, V'_{emf} is in micro-volts, B is in tesla and B' is in milli-gauss.

$$V'_{emf} = 10^6 V_{emf} \quad 5.1-4$$

$$B' = 10^{12} B \quad 5.1-5$$

Substituting these equations into 5.1-2 leads to the result:

$$V'_{emf} = (A \times 10^{-6}) \frac{dB'}{dt} \quad 5.1-6$$

If B' is a sinusoidal field, then $B' = B_0 \sin 2\pi ft$. Substituting this into 5.1-6 yields :

$$V'_{emf} = (2\pi A \times 10^{-6}) \cdot f \cdot B_0 \cos 2\pi ft$$

$$\text{or} \quad V'_{emf} = S_a \cdot f \cdot B_0 \cos 2\pi ft \quad 5.1-7$$

$S_a \triangleq 2\pi A \times 10^{-6}$ is called the absolute sensitivity when V'_{emf} is

measured in micro-volts, B_0 in milli-gauss and frequency in Hertz. At a frequency of 1 Hz, a field of 1 milli-gauss (10^{-8} Gauss) will induce a potential of 1 micro-volt and the sensitivity will be 1 Caner.

$$1 \text{ Caner} = 1 \mu\text{V}/(\text{m}\gamma \cdot \text{Hz})$$

Now two equations can be written, one for the air core coil system and the other for the Mu-metal core coil system by substituting 5.1-7 into 5.1-3. The superscript "1" is for the air core and "2" is for the Mu-metal core.

$$V_o^{(1)} = S_a^{(1)} \cdot f \cdot B_0 \cos 2\pi ft \cdot G^{(1)} \cdot \frac{R_i^{(1)}}{R_i^{(1)} + R^{(1)}} \cdot H^{(1)}(f) \quad 5.1-8$$

$$V_o^{(2)} = S_a^{(2)} \cdot f \cdot B_0 \cos 2\pi ft \cdot G^{(2)} \cdot \frac{R_i^{(2)}}{R_i^{(2)} + R^{(2)}} \cdot H^{(2)}(f) \quad 5.1-9$$

An important result occurs when the ratio of these equations is taken. This is given by :

$$\frac{V_o^{(2)}}{V_o^{(1)}} = \frac{S_a^{(2)}}{S_a^{(1)}} \cdot \frac{G^{(2)}}{G^{(1)}} \cdot \frac{R_i^{(2)}}{(R_i^{(2)} + R^{(2)})} \cdot \frac{(R_i^{(1)} + R^{(1)})}{R_i^{(1)}} \cdot \frac{H^{(2)}(f)}{H^{(1)}(f)} \quad 5.1-10$$

As the agreement between computer analysis and laboratory analysis has been very good for the work concerning the bridge method and the secondary coil method, the frequency response of the air core coil system is determined by programming the circuit parameters on the computer. The circuit diagram for this system is shown in Fig. 5.1-1. $H^{(1)}(f)$ can be expressed as the product of two transfer functions. The first one is

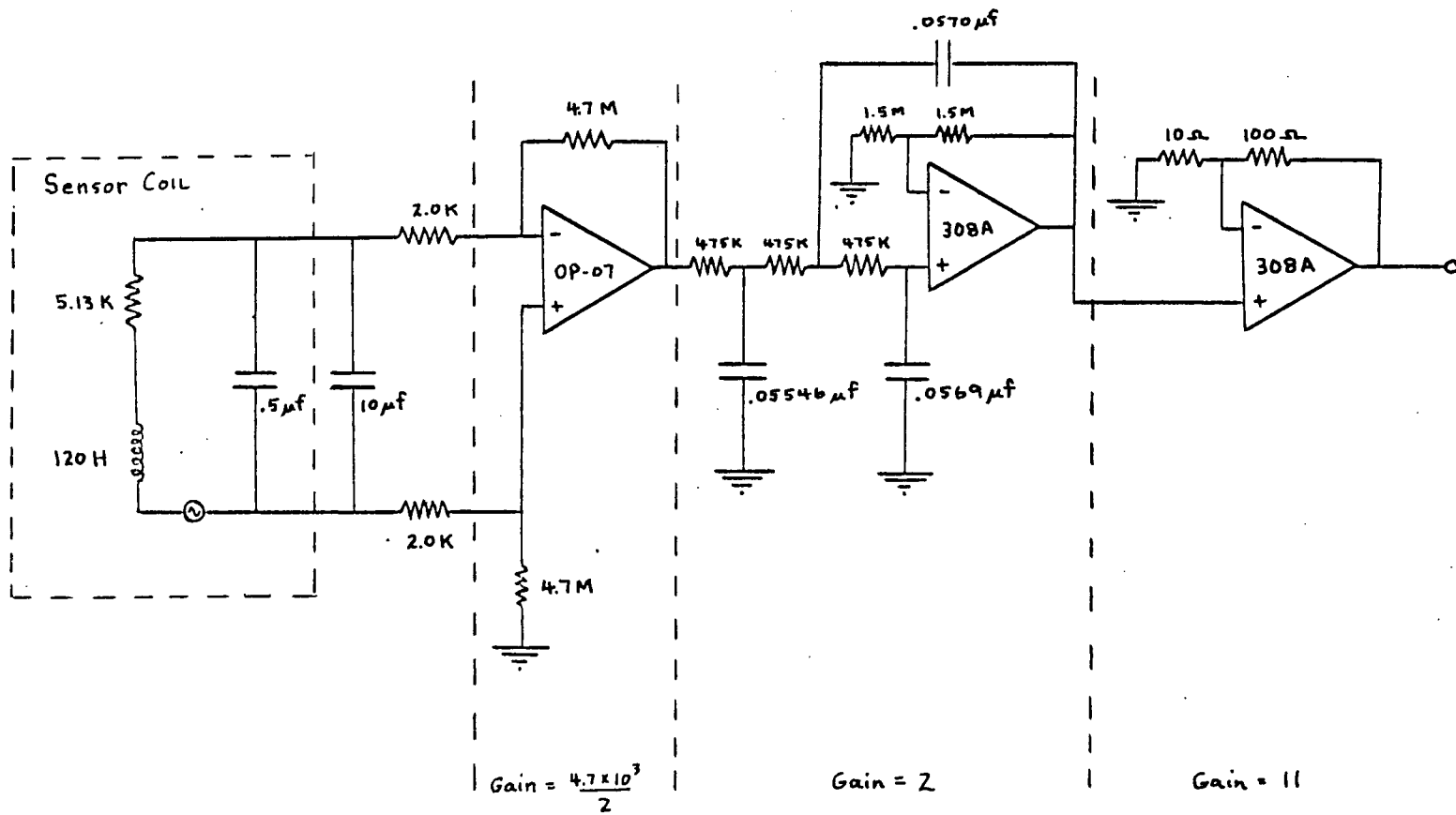
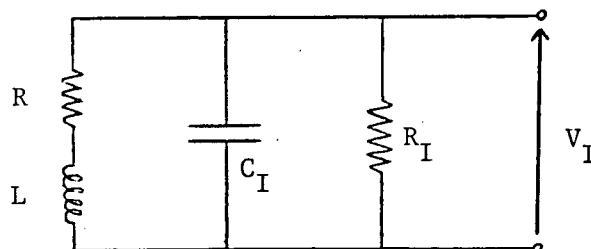


Fig. 5.1-1 Circuit diagram for the air core system

$H_1^{(1)}(f)$, approximately of a Butterworth type. The second is the transfer function of the third order low pass filter, $H_2^{(1)}(f)$.

In order to determine $H_1^{(1)}(f)$, consider the following figure :



From this diagram :

$$\frac{V_I}{E} = \frac{Z}{(Z + R + j\omega L)}$$

$$\text{where: } Z = \frac{R_I}{1 + j\omega C_I R_I}$$

Normalizing V_I/E to one at d.c., $H_1^{(1)}(f)$ becomes :

$$H_1^{(1)}(f) = \frac{(R + R_I)}{R_I} \cdot \frac{Z}{(Z + R + j\omega L)}$$

$H_2^{(1)}(f)$ is derived in Appendix 3. Therefore, the transfer function for the air core coil system, normalized to one at d.c. is :

$$H^{(1)}(f) = H_1^{(1)}(f) \cdot H_2^{(1)}(f)$$

This result was programmed on the computer. The frequency response curve which was determined is shown in Fig. 5.1-2.

As the frequency response curves for both the air core and the Mu-metal core systems are flat in the low frequency range, the terms $H^{(1)}(f)$ and $H^{(2)}(f)$ in 5.1-10 are both equal to one.

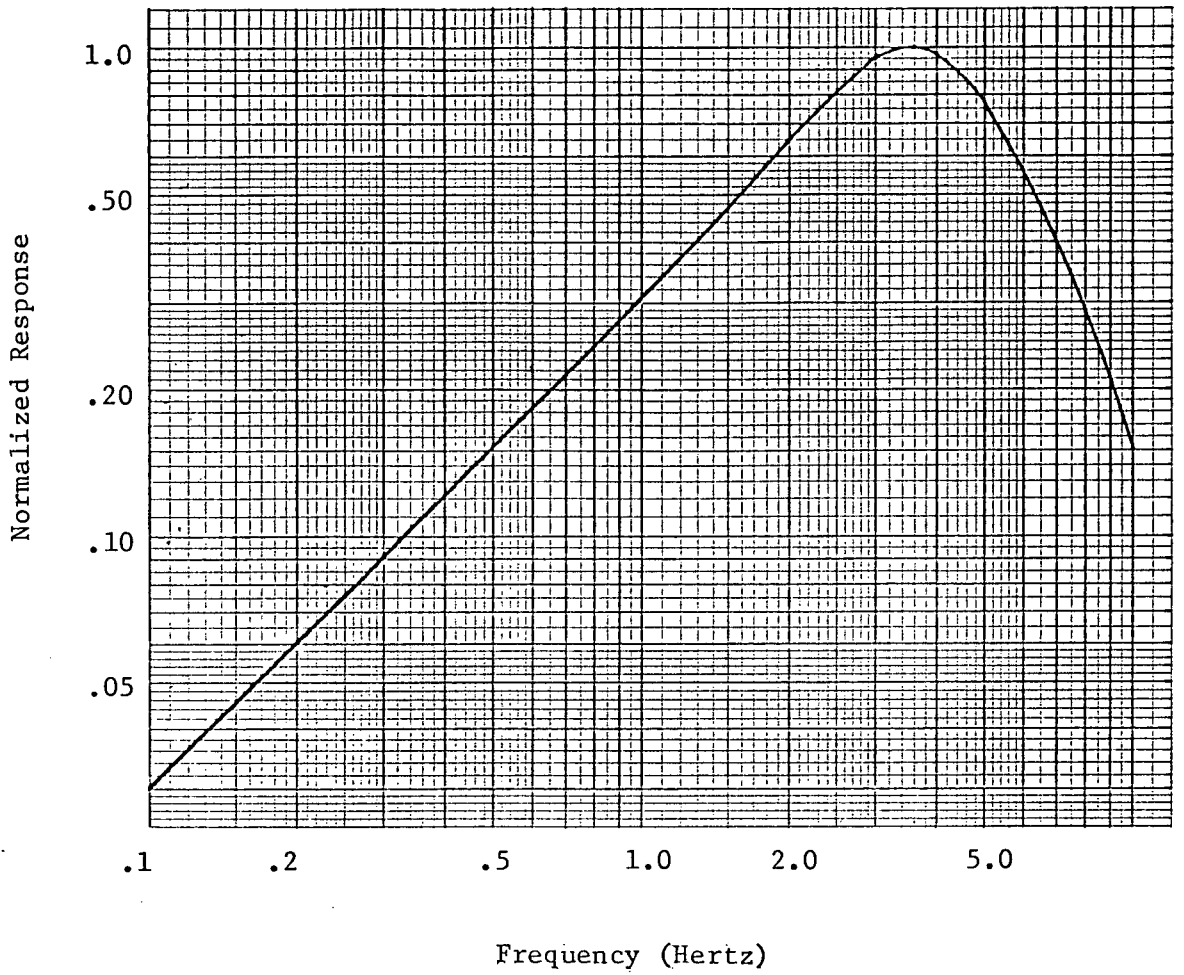


Fig. 5.1-2 Computer simulated frequency response of the air core coil system

The absolute sensitivity of the air coil, $S_a^{(1)}$, is easily determined from its geometry and turn number. In order to find the inner radius of the coil, the following method was used.

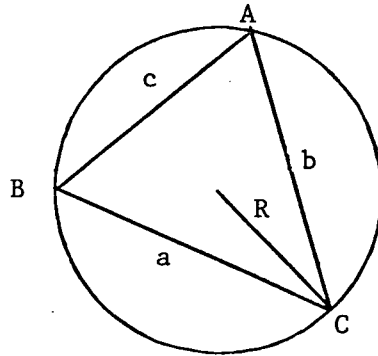


Fig. 5.1-3 Method to determine the inner radius of a large coil

Three measurements were taken along the inner circumference of the coil as shown in Fig. 5.1-3. From the law of cosines, the angle C is given by :

$$C = \cos^{-1} \left(\frac{a^2 + b^2 - c^2}{2ab} \right)$$

Then, an equation was used for a circumscribed triangle in order to find the radius. This equation is :

$$R = \frac{a}{2 \sin A} = \frac{b}{2 \sin B} = \frac{c}{2 \sin C}$$

After finding the inner radius, the outer radius was determined by adding the thickness of the coil to it. From this approach, $R_{\text{inner}} = 74.511$ cm and $R_{\text{outer}} = 75.702$ cm. Now the absolute sensitivity can be found.

$$S_a^{(1)} = 2\pi A \times 10^{-6}$$

$$\text{or } S_a^{(1)} = 2\pi \left[\pi N \frac{(r_i^2 + r_o r_i + r_o^2)}{3} \right] \times 10^{-6}$$

where r_i and r_o are the inner and outer radii, respectively. Substituting in the numbers leads to $S_a^{(1)} = .0557$ Caner $\pm .2\%$.

The ratio $V_o^{(2)}/V_o^{(1)}$ can be determined by measuring the amplitude of the signal from the air core and the Mu-metal core systems when a sinusoidal micropulsation event occurs. The output signals from the event used is shown in Fig. 5.1-4.

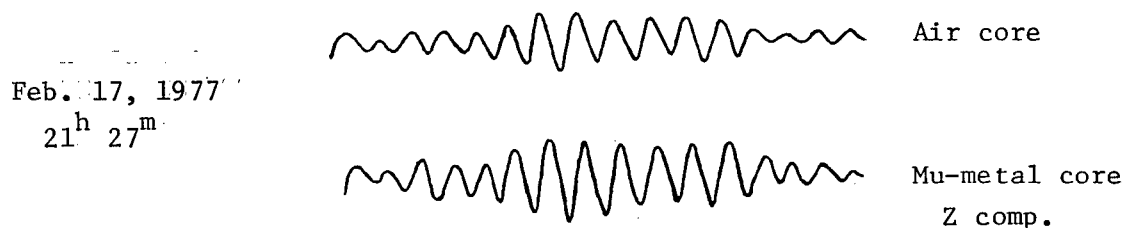


Fig. 5.1-4 The micropulsation event used for the absolute calibration

Peak-to-peak measurements were made from microfilm by using a travelling microscope. The ratios were taken with the result of :

$$\frac{V_o^{(2)}}{V_o^{(1)}} = 1.41 \pm .74\% \quad \text{at } .245 \text{ Hz} \pm 1.6\%$$

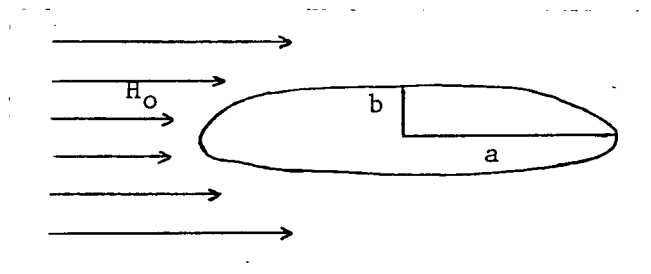
Finally, the remaining parameters of 5.1-10 have the following values :

$$\begin{aligned}
 G(1) &= 5.097 \cdot 10^4 \pm 1\% & G(2) &= 4.01 \cdot 10^4 \pm 1\% \\
 R_i(1) &= 4.0 \text{ K}\Omega \pm 1\% & R_i(2) &= 7.21 \text{ K}\Omega \pm 4\% \\
 R(1) &= 5130 \Omega \pm 1\% & R(2) &= 1831 \Omega \pm 1\%
 \end{aligned}$$

Note that $R_i(2)$ is different from $R_0 = 7.5 \text{ K}\Omega$ (p.55) because another amplifier unit was used for the field observation. The value of $S_a(2)$ according to 5.1-10 is .0548 Caner $\pm 6.4\%$.

V-2 A Theoretical Approach to the Absolute Sensitivity

The absolute sensitivity can be dealt with from a theoretical point of view. Consider a prolate spheroid with semiprinciple axes a, b immersed in a magnetic field of strength H_0 .



The Mu-metal core of the sensor is in reality a cylinder, but approximating the cylinder as a prolate spheroid is reasonably accurate and saves a great amount of mathematical difficulty. The results of an analysis shown in the book by Stratton (1940) indicates that the magnetic field strength anywhere inside the cavity is given by :

$$H = \frac{H_0}{1 + \frac{ab^2}{2} (\mu - 1) A}$$

5.2-1

where:
$$A = \frac{1}{a^3 e^3} \left(-2e + \ln \frac{1+e}{1-e} \right)$$

$$e = \sqrt{1 - \frac{b^2}{a^2}}$$

The magnetic field follows from $B = \mu \mu_0 H$ where μ is the relative permeability and μ_0 the permeability of free space. In MKS units, $\mu_0 = 4\pi \times 10^{-7}$ Henry/meter. μ is non-dimensional and is the permeability of the metal from which the core is made. By letting $B_0 = \mu_0 H_0$, it follows that :

$$B = \frac{\mu}{1 + \frac{ab^2}{2} (\mu - 1) A} B_0 \quad 5.2-2$$

The total flux Φ through the coil follows from 5.1-1.

$$\Phi = \pi b^2 \cdot B \cdot N$$

Or, substituting for B according to 5.2-2 :

$$\Phi = \frac{\mu \cdot \pi b^2 \cdot N}{1 + \frac{ab^2}{2} (\mu - 1) A} B_0 \quad 5.2-3$$

Let

$$S = \frac{\mu \cdot \pi b^2 \cdot N}{1 + \frac{ab^2}{2} (\mu - 1) A} \quad 5.2-4$$

Then $\Phi = SB_0$. The electromotive force generated by the changing flux would be :

$$V = \frac{d\Phi}{dt} = S \frac{dB_0}{dt}$$

Comparing this to 5.1-7, it is seen that S represents a theoretical sensitivity. Expressing S in units of Caner, the sensitivity becomes :

$$S_{\text{theor}} = 2\pi \times 10^{-6} S$$

For a Mu-metal core, μ is of the order of 10^5 . If a restriction is put on the ratio of the lengths of the semiprinciple axes:

$$\frac{b}{a} > \frac{1}{200}$$

then the denominator of the expression 5.2-4 for S can be reduced to a simpler form.

$$1 + \frac{\alpha b^2}{2} (\mu - 1) A \approx \frac{\alpha b^2 \mu}{2} A \quad 5.2-6$$

The error of this approximation is less than 8%. The expression for sensitivity reduces to :

$$S = \frac{2\pi N}{\alpha A} \quad 5.2-7$$

The expression 5.2-1 for A can also be simplified. If $\frac{b}{a} \ll \frac{1}{5}$, then $e \approx 1$ and A becomes :

$$A = \frac{1}{\alpha^3 e^3} \left[-2 + \ln 2 - \ln(1 - e) \right] \quad 5.2-8$$

By the binomial expansion :

$$e = \sqrt{1 - \frac{b^2}{a^2}} \approx \frac{1}{2} \frac{b^2}{a^2}$$

Then 5.2-8 reduces to :

$$A = \frac{1}{\alpha^3} \ln \frac{4a^2}{e_0^2 b^2} \quad 5.2-9$$

where $e_0 = 2.71828$. The final simplified expression for

sensitivity follows from 5.2-9, 5.2-5 and 5.2-6.

$$S_{\text{approx}} = \frac{2\pi^2 N a^2}{\ln\left(\frac{2a}{e_0 b}\right)} \times 10^{-6} \quad \text{Caner} \quad 5.2-10$$

The importance of this expression is that the sensitivity of the sensor coil is primarily dependent upon the number of windings, N , and the length of the coil, a . The overall weight of the sensor could be reduced by using lighter gauge wire and a thinner core. The length and turn number could be adjusted to obtain the desired level of sensitivity.

In spite of many approximations, the agreement amongst the theoretical and experimental results of 5.2-10, 5.2-5 and $S_a^{(2)}$ of 5.1-10 is quite good*. The values are shown below :

$$S_a^{(2)} = .0548 \text{ Caner} \pm 6.4\%$$

$$S_{\text{theor}} = .0583 \text{ Caner}$$

$$S_{\text{approx}} = .0587 \text{ Caner}$$

These results imply that the approximate theoretical expression for the absolute sensitivity, eq. 5.2-10, can be reliably used to aide in the design of future sensor coils.

Another interesting observation which has been made as a result of this analysis is that the ratio a/b cannot be increased without bound unless an undesirable effect begins to take place. When $\frac{a}{b} > 100$, S_{theor} and S_{approx} start to diverge by about 2% and the agreement becomes worse as a/b becomes larger. There is an important reason behind this which can be

* For absolute calibration according to the bridge method, see Appendix IV.

unfolded by once again taking a look at 5.2-2. B can be re-expressed in terms of a demagnetization coefficient N_d .

$$B = \frac{\mu}{1 + N_d(\mu - 1)} B_0 \quad 5.2-11$$

$$N_d = \frac{ab^2}{2} A$$

It can be seen that the inverse of the demagnetization coefficient is the permeability which leads to the sensitivity given by eq. 5.2-10. Writing

$$\mu_1 = \frac{1}{N_d} = \frac{2}{ab^2 A} \quad 5.2-12$$

it is seen with the help of 5.2-9 :

$$\mu_1 = \frac{a^2}{b^2} \frac{1}{\ln\left(\frac{2a}{e_0 b}\right)} \quad 5.2-13$$

Note that this is dependent upon the geometry of the core but not the properties of the metal. μ_1 is dependent upon the ratio a/b . By making the substitution 5.2-12 into 5.2-13, it is seen that :

$$B = \mu_{\text{eff}} B_0 \quad 5.2-14$$

$$\text{where: } \mu_{\text{eff}} = \frac{\mu \mu_1}{\mu_1 + \mu - 1}$$

For the most recent Mu-metal core coil used for this research, $a=45.72$ cm and $b=31.02$ cm (see Table I-1). This

leads to a value for μ_1 of 595. Since $\mu = 10^5$, the inequality $\mu \gg \mu_1$ is satisfied. Then by 5.2-14, $\mu_{\text{eff}} \approx \mu_1$. This is a desirable result because the effective permeability of the core is dependent upon its geometry. When $a/b \approx 100$, the inequality $\mu \gg \mu_1$ begins to weaken. When $a/b = 1000$, $\mu_1 = 1.5 \times 10^5$ and μ_{eff} is no longer dependent principally upon μ . The permeability of the metal, μ , becomes equally as important. This is not a desirable result as the permeability of a metal is not always constant. It may change significantly according to environmental conditions such as temperature and stress upon the metal. A plot of μ_1 as a function of a/b can be seen in Fig. 5.2-1.

The conclusion of this analysis is that eq. 5.2-10 will give a good indication of the sensitivity of a cylindrically shaped sensor coil provided $5 \leq \frac{a}{b} \leq 150$.

Note:

The value of b at the bottom of p. 78 is not simply the inner diameter of the coil windings. It actually denotes an effective radius resulting from the cross-sectional area of the Mu-metal core itself. The core consists of approximately 48 rectangular strips. The cross-sectional area of one strip is $(3/4")(.014") = (1.905 \text{ cm})(.03556 \text{ cm}) = .06774 \text{ cm}^2$. If there are 48 strips, then the total cross-sectional area is 3.252 cm^2 . The effective radius for this area is $\sqrt{3.252/\pi} = 1.02 \text{ cm}$.

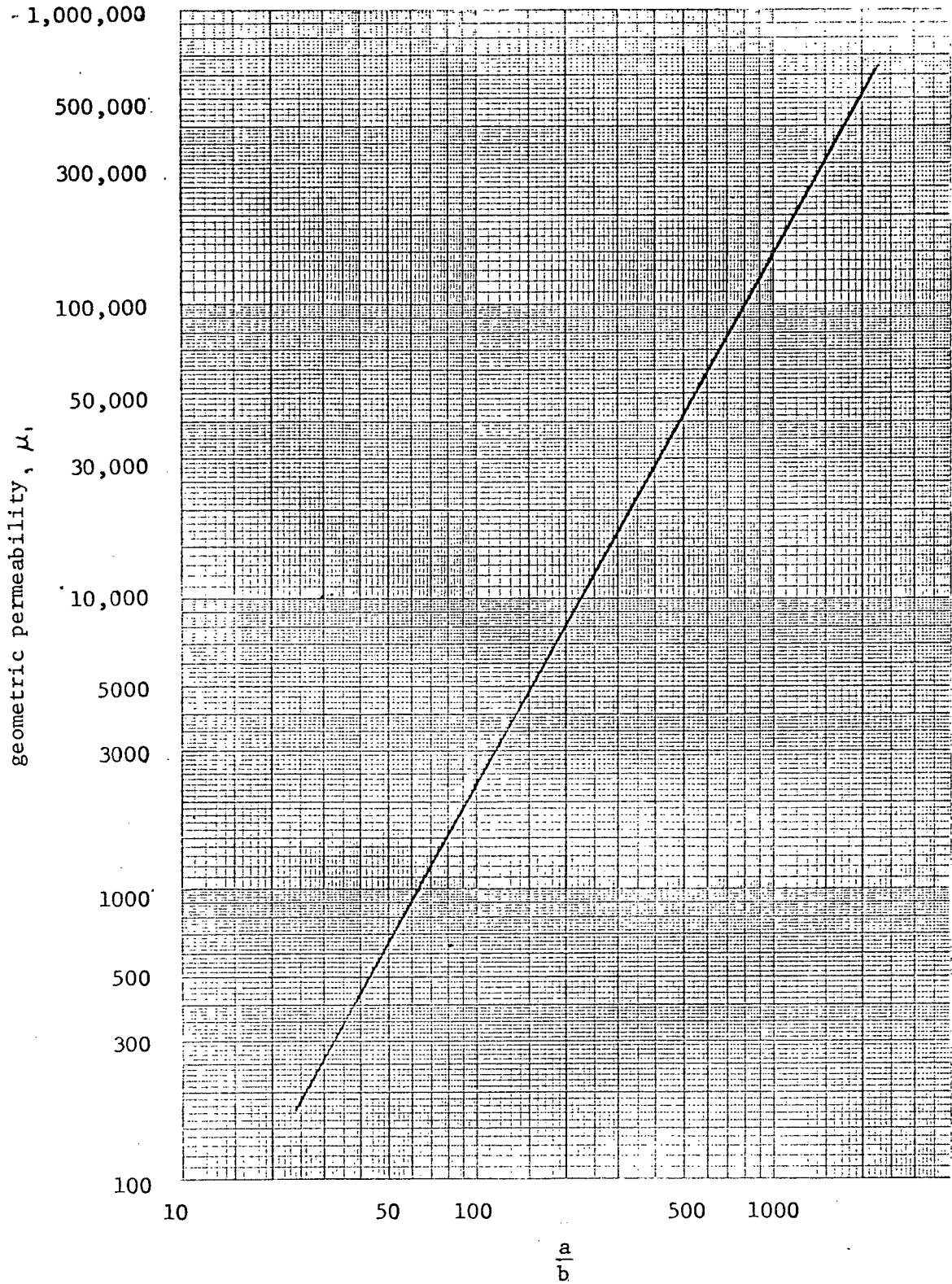


Fig. 5.2-1 The dependence of the geometric permeability μ , upon the ratio of the lengths of the semiprincipal axes of a prolate spheroid, a/b

CHAPTER VISUMMARY AND CONCLUDING REMARKS

Many useful results have been obtained from the investigations carried out in this thesis. These results fall into two categories.

One category is concerned with improvements in the design of the magnetometer system. As described in Chapter II, use can be made of a Butterworth filter rather than a notch filter to reduce 60 Hz noise. This guarantees a flat response in the low frequency range and requires only two matched electrical components rather than six carefully matched components. In Chapter V, which was concerned with the absolute calibration, it was shown that the sensitivity of the sensor coil is primarily dependent upon the number of windings and the length of the coil. The overall weight of the sensor could be reduced by using lighter gauge wire and a thinner core. However, for optimum performance, the ratio of the length to the diameter of the core must be within a specific range. One of the reasons for not being able to increase sensitivity ad infinitum is that thermal agitations at the atomic level induce small currents in the sensor and other electrical components. This is known as Johnson noise.

The second category concerns the calibration procedure. Two methods were investigated in great detail, the bridge method and the secondary coil method. It was determined that both methods can produce reliable relative frequency response

curves. An advantage of the bridge method over the secondary coil method is that only one cable is needed between the sensor coil and the remaining electronics, rather than two. For this reason, the bridge method will probably be used for future calibrations.

The absolute calibration was successfully performed by comparing the Mu-metal core system to a previously calibrated air core system. A theoretical approach to the absolute calibration was discussed which agreed well, considering all of the approximations made, with the laboratory results. This theoretical approach may be used to obtain a good indication of the sensitivity of a cylindrically shaped coil before a laboratory analysis is performed.

APPENDIX 1

METHODS OF DETERMINING THE INDUCTANCE AND CAPACITANCE OF A
COIL WITH FINITE RESISTANCE

It is not a trivial problem to determine the inductance and capacitance of a coil which has a finite resistance. The sensor coils used with the magnetometer system all have the equivalent circuit of Fig. A.1-1.

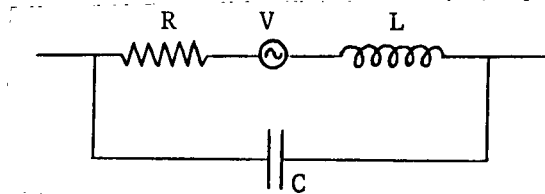


Fig. A.1-1 Equivalent circuit of a sensor coil

A meter which is normally used to measure an inductance or a capacitance operates on the principle that $R=0$. For the sensor coils, R is of the order of a few thousand ohms. Because of this, other less straight forward techniques must be employed to determine L and C . This appendix is a compilation of those techniques which were used in the laboratory. It is safe to measure coil resistance by using an ohm meter.

Methods of Determining L

The most reliable method of determining L follows from wiring a signal generator, the coil and a load resistor in

series.

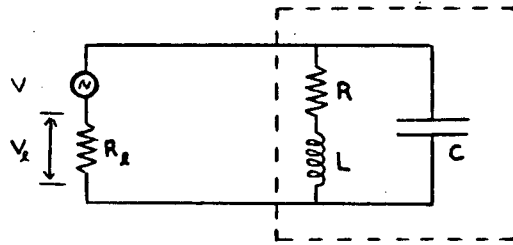


Fig. A.1-2 First method of determining L

The signal generator must produce a sinusoidal signal of a frequency which is low enough such that :

$$\left| \frac{1}{j\omega C} \right| \gg |R + j\omega L| \quad \text{A.1-1}$$

Then the presence of the capacitor can be ignored in the circuit analysis. For the R-L -R_x loop, the following equation is true:

$$\frac{V_x}{V} = \frac{R_x}{\sqrt{R^2 + \omega^2 L^2}}$$

Rearranging this into a different form :

$$\left(\frac{V}{V_x} \right)^2 = \left(\frac{R}{R_x} \right)^2 + \left(\frac{L}{R_x} \right)^2 \omega^2 \quad \text{A.1-2}$$

Thus, a plot of $(V/V_x)^2$ versus ω^2 is a straight line with slope $(L/R_x)^2$.

Another circuit which can be used for determining L is shown in Fig. A.1-3. This is identical to the previous circuit except that the signal generator produces a square

wave instead of a sinusoid.

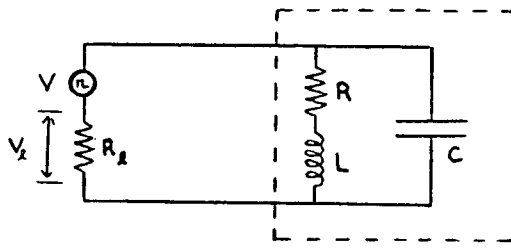


Fig. A.1-3 Second method of determining L.

In order for this method to produce the desired results, there are two conditions which must be met. These are :

$$\frac{R}{R_x} \gg 1$$

A.1-3

$$\frac{L}{R} \gg CR_g$$

Then the scope picture across R_x will show an increasing and a decreasing exponential. By measuring the time which it takes for V_x to obtain one half of the final value, the inductance can be found from :

$$\tau_{\frac{1}{2}} = \frac{L}{R} \ln 2$$

A.1-4

This method of determining L is reliable, but in practice it is difficult to obtain better than one significant figure of accuracy because the time interval of $\tau_{\frac{1}{2}}$ is not easy to measure using available scopes or chart recorders.

Methods of Determining C

The most reliable method to determine C follows by again using the circuit of Fig. A.1-2, but this time at high frequencies. The condition which needs to be met is :

$$|R + j\omega L| \gg \left| \frac{1}{j\omega C} \right| \quad \text{A.1-5}$$

Also, another necessary condition is :

$$\left| \frac{1}{j\omega C} \right| \gg R_x \quad \text{A.1-6}$$

When the frequency becomes high enough, $|j\omega L|$ becomes so large that nearly all the current passes through the capacitor. If V_x is the voltage drop across R_x , the capacitance C follows from A.1-7.

$$C = \frac{V_x}{\omega V R_x} \quad \text{A.1-7}$$

On the plot of $\log \omega$ versus $\log V_x$, this equation is valid on the 45° sloping line to the right of the resonance point.

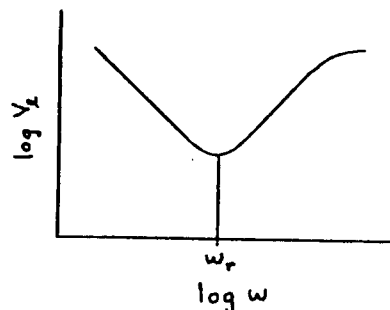


Fig. A.1-4 The anti-resonance point

ω_r is called the anti-resonance frequency. The coil

inductance and capacitance are related to ω_r according to A.1-8. This expression actually defines the resonance frequency, but the resonance point and the anti-resonance point are in this case essentially identical.

$$\omega_r = 1 / \sqrt{LC} \quad \text{A.1-8}$$

Thus, if ω_r and L are known, then C can be determined using A.1-8. If a capacitor is wired parallel to the coil in the circuit of Fig. A.1-2, then the resonance point will be shifted to a lower frequency according to A.1-9 where C_a is the additional capacitor.

$$\omega_r = 1 / \sqrt{L(C+C_a)} \quad \text{A.1-9}$$

Both L and C can be determined by shifting the resonance point as A.1-8 and A.1-9 are two equations with two unknowns. A practical difficulty with this approach is that as the resonance point is shifted to the lower frequencies, the trough of Fig. A.1-4 becomes shallower and ω_r more poorly defined.

A more complete review of these techniques for determining L and C may be found in Ueda and Watanabe (1975).

APPENDIX 2

THE TRANSFER FUNCTION OF THE AMPLIFIER SYSTEM

Both methods of calibration have in common the amplifier system which filters and amplifies the signal from the sensor coil. In order to make computer simulations of frequency response curves, the transfer function for the amplifier electronics must be determined.

A schematic for the amplifier is shown in Fig. A.2-1. The transfer function for each stage is given in Fig. A.2-2. The transfer function for all of the electronics of the amplifier system is then :

$$T(j\omega) = \frac{1}{\left(1 + j\frac{\omega}{\omega_c}\right)} \cdot \frac{(\omega)^2 + \omega_N^2}{(j\omega)^2 + j4\omega_N\omega + \omega_N^2} \cdot \frac{\omega_c^2}{(j\omega)^2 + j2\omega_c\omega + \omega_c^2}$$

A.2-1

where: $\omega_N = \frac{1}{RC} = \frac{1}{(1.206 \text{ K}\Omega)(2.2 \mu\text{f})}$

$$\omega_c = 12\pi$$

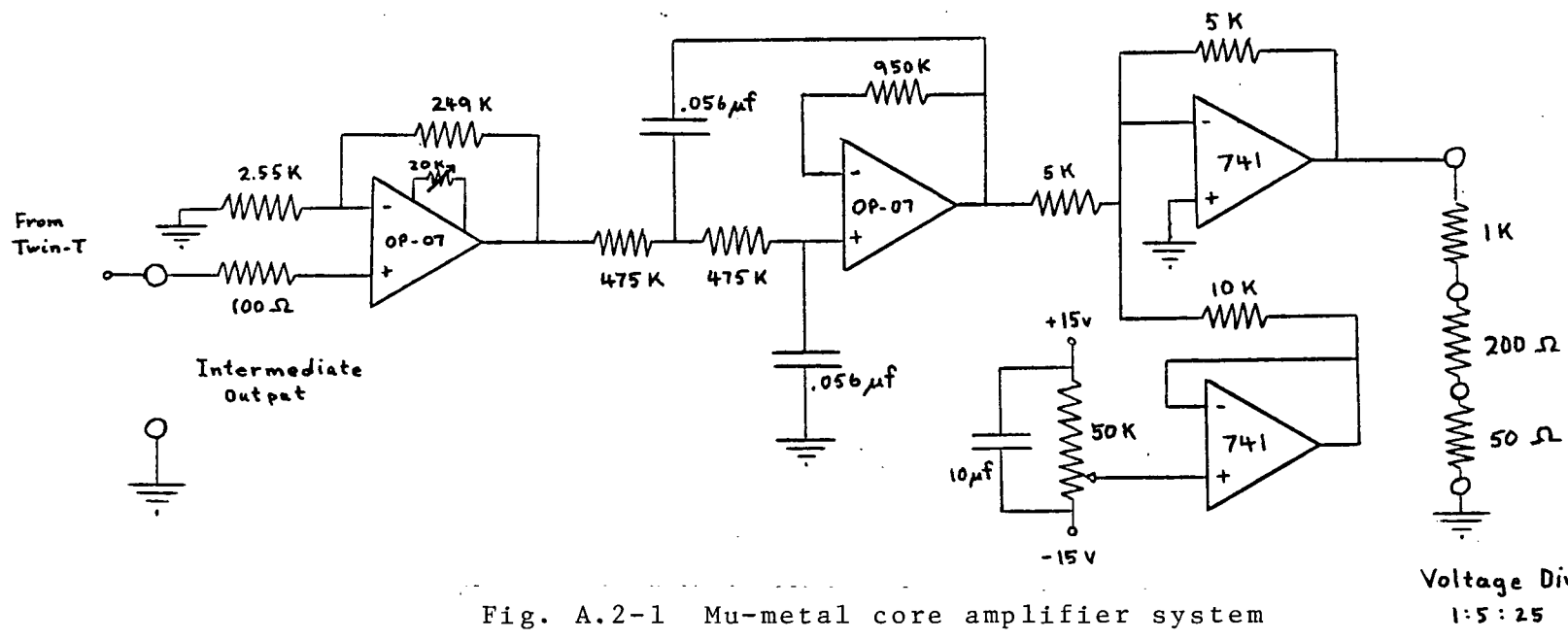
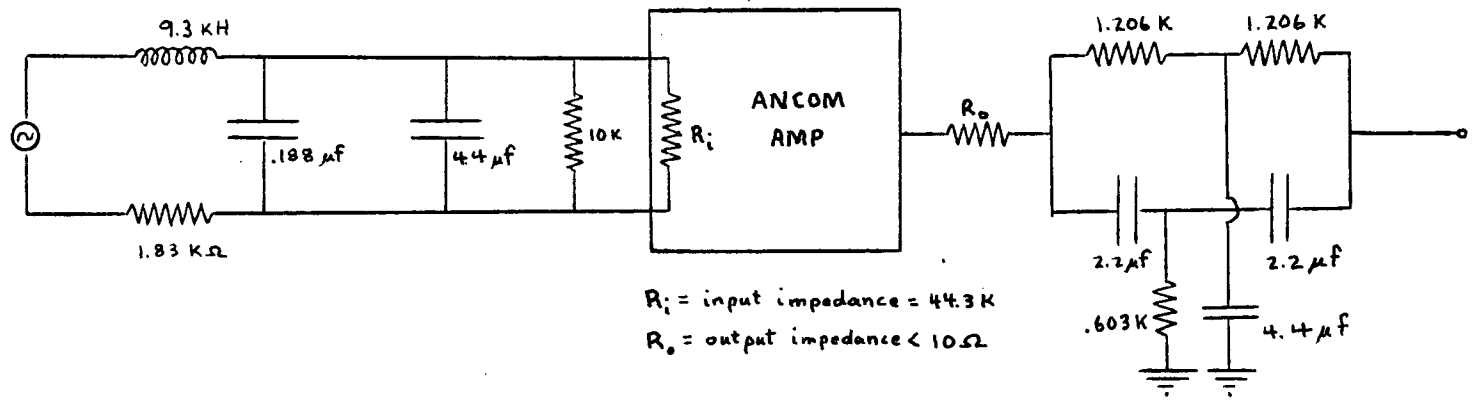
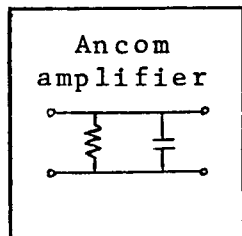


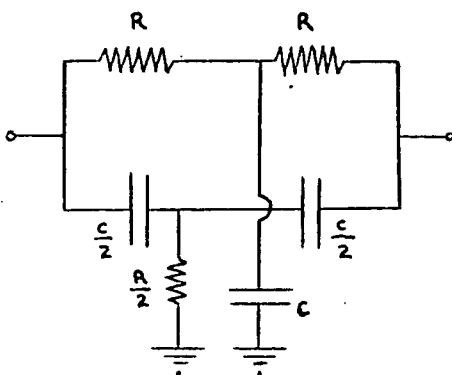
Fig. A.2-1 Mu-metal core amplifier system

Fig. A.2-2 Transfer functions for filters of the Mu-metal core amplifier system



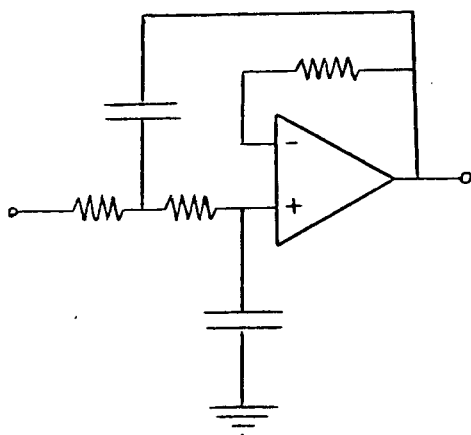
$$\frac{1}{1 + j \frac{\omega}{\omega_c}}$$

$$\omega_c = 12\pi^*$$



$$\frac{(j\omega)^2 + \omega_N^2}{(j\omega)^2 + j4\omega_N\omega + \omega_N^2}$$

$$\omega_N = \frac{1}{RC}$$



$$\frac{\omega_c^2}{(j\omega)^2 + j2\omega\omega_c + \omega_c^2}$$

$$\omega_c = 12\pi$$

* Butterworth filter of 1st degree. Corner frequency = 6 Hz.

APPENDIX 3

THE TRANSFER FUNCTION FOR THE THIRD ORDER LOW PASS FILTER

The circuit diagram for the third order low pass filter which is used as a part of the air core magnetometer system electronics is shown in Fig. A.3-1.

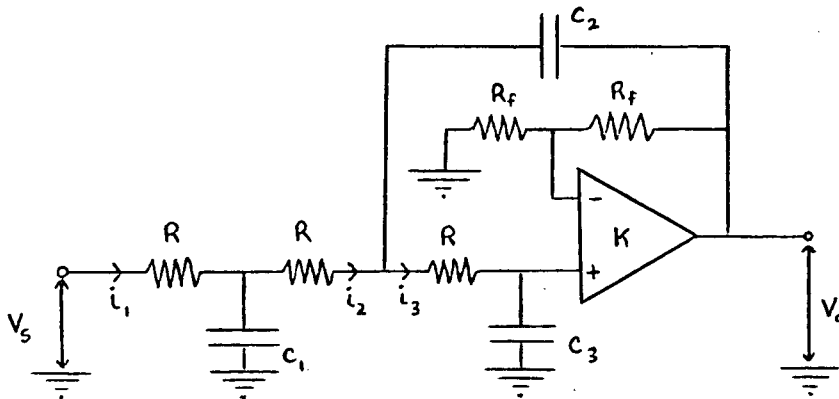


Fig. A.3-1 The third order low pass filter

Four fundamental equations which can be written are given by equations A.3-1 through A.3-4.

$$V_s = i_1 R + (i_1 - i_2) Z_1 \quad \text{A.3-1}$$

$$V_o = (i_3 - i_2) Z_2 - i_2 R + (i_1 - i_2) Z_1 \quad \text{A.3-2}$$

$$-(i_1 - i_2) Z_1 + i_2 R + i_3 R + i_3 Z_3 = 0 \quad \text{A.3-3}$$

$$V_o = K i_3 Z_3, \quad K = 2 \quad \text{A.3-4}$$

For these equations, Z_1 , Z_2 and Z_3 are the complex impedances of C_1 , C_2 and C_3 . Using the top three equations, the matrix equation that results is :

$$\begin{pmatrix} (R+Z_1) & -Z_1 & 0 \\ Z_1 & -(Z_2+R+Z_1) & Z_2 \\ -Z_1 & (Z_1+R) & (R+Z_3) \end{pmatrix} \begin{pmatrix} i_1 \\ i_2 \\ i_3 \end{pmatrix} = \begin{pmatrix} V_s \\ V_o \\ 0 \end{pmatrix} \quad \text{A.3-5}$$

The solution for I_3 is :

$$I_3 = \frac{2RV_o Z_1 + V_o R^2 + V_s Z_1 Z_2}{(R+Z_1)(2Z_2 R + Z_2 Z_3 + R^2 + Z_3 R) + RZ_1(Z_2 + R + Z_3)} \quad \text{A.3-6}$$

Making the substitution for V_o from A.3-4 into A.3-6 and then solving for the ratio V_o/V_s leads to :

$$\frac{V_o}{V_s} = \frac{Z_1 Z_2 Z_3 K}{(R+Z_1)(2Z_2 R + Z_2 Z_3 + R^2 + Z_3 R) - RZ_3 K(2Z_1 + R) + RZ_1(Z_2 + R + Z_3)} \quad \text{A.3-7}$$

The final substitutions to make are for Z_1 , Z_2 and Z_3 into A.3-7 where :

$$\begin{aligned} Z_1 &= (j\omega C_1)^{-1} \\ Z_2 &= (j\omega C_2)^{-1} \\ Z_3 &= (j\omega C_3)^{-1} \end{aligned}$$

After rearrangement of terms, this leads to the result of A.3-8 where $s=j\omega$.

$$\frac{V_o}{V_s} = \frac{K}{\left[s^3 C_1 C_2 C_3 R^3 + s^2 \{ 2R^2 C_2 C_3 + R^2(1-K)C_1 C_2 + 2R^2 C_1 C_3 \} + s \{ 3RC_3 + 2R(1-K)C_2 + RC_1 \} + 1 \right]} \quad \text{A.3-8}$$

Let H_2 be the transfer function of the third order low pass filter normalized to one at d.c. Then :

$$H_2 = \frac{1}{K} \frac{V_o}{V_s} \quad \text{A.3-9}$$

APPENDIX 4-THE ABSOLUTE CALIBRATION ACCORDING TO THE BRIDGE METHOD-

Using the development of the bridge method as discussed in III-2, a relationship can be derived between the time varying external magnetic field, B , and the emf generated in the sensor coil. This is a calculation of the absolute sensitivity as discussed in Chapter V.

Eq. 3.2-7 is a relationship between the driving voltage of the bridge and the flux through the coil. This result is:

$$\frac{E}{R_4} = \frac{N\phi}{L} \quad \text{A.4-1}$$

It is necessary to express ϕ in terms of H , and L in terms of coil geometry. For a solenoid of length ℓ and cross-section area A such that end effects are negligible, and closely wound with N turns of thin wire so that the winding resembles a current sheet, the two expressions for ϕ and L are :

$$\phi = \mu_0 k A H \quad \text{A.4-2}$$

$$L = \mu_0 k N^2 A / \ell \quad \text{A.4-3}$$

where μ_0 is the permeability of free space and k is the relative permeability. Substituting these two equations into A.4-1, the result is :

$$H = \frac{N}{\ell R_4} E \quad \text{A.4-4}$$

APPENDIX 4

THE ABSOLUTE CALIBRATION ACCORDING TO THE BRIDGE METHOD

Using the development of the bridge method as discussed in III-2, a relationship can be derived between the time varying external magnetic field, B , and the emf generated in the sensor coil. This is a calculation of the absolute sensitivity as discussed in Chapter V.

Eq. 3.2-7 is a relationship between the driving voltage of the bridge and the flux through the coil. This result is:

$$\frac{E}{R_4} = \frac{N\phi}{L} \quad \text{A.4-1}$$

It is necessary to express ϕ in terms of H , and L in terms of coil geometry. For a solenoid of length ℓ and cross-section area A such that end effects are negligible, and closely wound with N turns of thin wire so that the winding resembles a current sheet, the two expressions for ϕ and L are :

$$\phi = \mu_0 k A H \quad \text{A.4-2}$$

$$L = \mu_0 k N^2 A / \ell \quad \text{A.4-3}$$

where μ_0 is the permeability of free space and k is the relative permeability. Substituting these two equations into A.4-1, the result is :

$$H = \frac{N}{\ell R_4} E \quad \text{A.4-4}$$

The sensor used for the field observation (see Fig. 5.1-4) was not available to test in the laboratory so that a direct comparison cannot be made between the sensitivity as obtained from A.4-4 and the results on page 77. The different sensors are nearly identical, so the best that can be done at this point is to make the sensitivity calculation using another sensor.

At a frequency of 1 Hertz, an input signal to the bridge of .75 mV p-p caused an output from the amplifier of 13 V p-p. For $N=50,000$, $l=.9144\text{m}$ and $R=38787\Omega$, A.4-4 indicates that $B=\mu_0 H$, where $\mu_0=4\pi \times 10^{-7}$, is $13.3 \times 10^2 \text{ m}\gamma$. The output from the bridge or the input to the amplifier is $13.0\text{V}/2 \times 10^5 = 65\mu\text{V}$. To find the emf in the sensor coil, use can be made of eq. 3.4-6.

The following values are used:

$$R_1 = 1.83 \text{ K}\Omega$$

$$L_1 = 930 \text{ H}$$

$$C_1 = 4.4 \mu\text{f}$$

$$Z_5 = 44.3 \text{ K}\Omega \parallel 10 \text{ K}\Omega = 8.158 \text{ K}\Omega$$

$$R_4 = 38.8 \text{ K}\Omega$$

This indicates that the ratio of the output from the bridge to the emf in the sensor coil is .771. Therefore, the emf in the sensor coil is $65\mu\text{V}/.771 = 84.3\mu\text{V}$. The sensitivity is then :

$$S = \frac{V_{\text{coil}}}{B} = \frac{84.3 \mu\text{V}}{13.3 \times 10^2 \text{ m}\gamma} = .063 \text{ Caner}$$

This is a reasonable result when it is compared to the results on page 77.

LIST OF REFERENCES CONSULTED

- Campbell, W.H. (1967)
Induction Loop Antennas for Geomagnetic Field Variation
Measurement, ESSA Technical Report, ERL 123-ESL 6.
- Kanasewich, E.R. (1973)
Time Sequence Analysis in Geophysics, Edmonton, The
University of Alberta Press, pp 170-186.
- Kollar, F. and Russell, R.D. (1966)
Seismometer Analysis Using an Electric Current Analog,
BSSA, 56, 1193-1205.
- Lewis, W.E. and Pryce, D.G. (1965)
The Application of Matrix Theory to Electrical Engin-
eering, London, E. & F.N. Spon Ltd, pp 141-171.
- Schwartz, M. (1972)
Principles of Electrodynamics, San Francisco, McGraw-
Hill Inc.
- Slurzberz, M. and Osterheld, W. (1944)
Electrical Essentials of Radio, McGraw-Hill Inc.,
pp. 269-303.
- Stratton, J.A. (1941)
Electromagnetic Theory, New York and London, McGraw-Hill
Inc.
- Ueda, H. (1975)
University of British Columbia, Geophysics,
M.Sc. Thesis.
- Ueda, H. and Watanabe, T. (1975)
Comments on the Anti-Resonance Method to Measure the
Circuit Constants of a Coil Used as a Sensor of an Induc-
tion Magnetometer, The Science Reports of the Tohoku
University, Series 5, Geophysics, Vol. 22, No. 3-4,
pp 129-135.
- Ueda, H. and Watanabe, T. (1975)
Several Problems about Sensitivity and Frequency Response
of an Induction Magnetometer, The Science Reports of the
Tohoku University, Series 5, Geophysics, Vol. 22, No. 3-4,
pp. 107-127.